STRUCTURAL HEALTH MONITORING OF A HIGH SPEED NAVAL VESSEL USING AMBIENT VIBRATIONS

A Thesis
Presented to
The Academic Faculty

By

Steven Paul Huston

In Partial Fulfillment
of the Requirements for the Degree
Master of Science in Mechanical Engineering

Georgia Institute of Technology

May, 2010

Structural Health Monitoring of a High Speed Naval Vessel Using Ambient Vibrations

Approved by:

Dr. Karim Sabra, Advisor
School of Mechanical Engineering
Georgia Institute of Technology

Dr. Massimo Ruzzene
School of Aerospace Engineering
Georgia Institute of Technology

Dr. Yang Wang
School of Civil and Environmental Engineering
Georgia Institute of Technology

Date Approved: March 5, 2010

ACKNOWLEDGEMENTS

I would like to gratefully acknowledge the guidance provided to me by my advisor, Dr. Karim Sabra, who has patiently, knowledgeably, and thoroughly guided me in the fields of seismology and acoustics. His knowledge and experience have been instrumental to the preparation of this paper and to my Master's degree as a whole.

Much of the details of this study, including the actual testing data that was central to my research, were provided by the Naval Surface Warfare Center, Carderock Division. Without this information, this study would not have been possible.

Finally, I wish to acknowledge my family, who has encouraged my continued pursuit of education. My parents have provided an example that has guided me throughout my education and life. My children, Anna and Bennett, will always be my heroes. And my wife, Jennifer, has supported me in countless ways in order to make this degree possible.

TABLE OF CONTENTS

LIST OF TABLES

LIST OF FIGURES

NOMENCLATURE

SHM: Structural Health Monitoring: the concept of determining a physical system's integrity through nondestructive methods.

DVI: Diffuse Vibration Interferometry: A method of SHM that involves estimating the structural response between two passive sensors using recordings of ambient vibrations.

FEA: Finite Element Analysis: A numerical technique of modeling physical systems to predict responses to inputs. For this study, the FEA referenced was used to evaluate structural responses to various inputs into the ship.

HSV: High Speed Vessel: The subject of this study, the HSV-2 *Swift*, is an aluminum-structured naval vessel.

SUMMARY

Traditional naval vessels with steel structures have the benefit of large safety factors and a distinct material endurance limit. However, as performance requirements and budget constraints rise, the demand for lighter weight vessels increases. Reducing the mass of vessels is commonly achieved by the use of aluminum or composite structures, which requires closer attention to be paid to crack initiation and propagation. It is rarely feasible to require a lengthy inspection process that removes the vessel from service for an extended amount of time. Structural health monitoring (SHM), involving continuous measurement of the structural response to an energy source, has been proposed as a step towards condition-based maintenance. Furthermore, using a passive monitoring system with an array of sensors has several advantages: monitoring can take place in real-time using only ambient noise vibrations and neither deployment of an active source nor visual access to the inspected areas are required.

Passive SHM on a naval vessel is not without challenge. The structures of ships are typically geometrically complex, causing scattering, multiple reflections, and mode conversion of the propagating waves in the vessel. And rather than a distinct and predictable input produced by controlled active sources, the vibration sources are hull impacts, smaller waves, and even onboard machinery and activity. This research summarizes findings from data collected onboard a Navy vessel and presents recommendations data processing techniques. The intent is to present a robust method of passive structural health monitoring for such a vessel using only ambient vibrations recordings.

CHAPTER 1: INTRODUCTION

Continued demands for increased performance, lower purchase price, and reduced operating costs have impacted the direction of modern naval development. A common method employed to meet these demands is to reduce the mass of vessels. This is often accomplished by using alternate materials and by incorporating lower safety factors into designs. Aluminum is one such material frequently used to accomplish weight savings in vessels, as compared to more traditional steel structures. The United States' naval vessel, High-Speed Vessel (HSV)-2 *Swift*, is an example of a ship utilizing aluminum structure. Its fundamental design is that of a wave-piercing catamaran.

Figure 1: High-Speed Vessel *Swift* (HSV-2) [1]

The HSV-2 *Swift* has the following dimensions [2]:

Overall length: 97.2 m (318.9 ft)
Waterline length: 92.0 m (301.8 ft)
Overall beam: 26.6 m (87.3 ft)
Beam at hulls: 4.5 m (14.7 ft)
Draft (fully loaded): 3.4 m (11.3 ft)
Maximum deadweight: 670 tonnes (1670 lton)
Lightship displacement: 1130 tonnes (1246 tons)
Maximum permitted displacement: 1800 tonnes (1984 tons)

The extruded members (including the majority of the ship's beam structures) are made of 6082-T6 aluminum, and the plate material (such as the decking and hull) utilizes 5383-H116/H321 aluminum [3].

A negative aspect to the use of aluminum in structures is the lack of a significant endurance limit. The strength of aluminum continuously decays with the application of repeated stress cycles. This precludes the use of universal standard stress limits to be used as a design guide. Small cracks can initiate and propagate into larger cracks especially quickly and without warning in a ship with an aluminum structure. Periodic inspection is the standard method of ensuring the soundness of an aluminum vessel. Such inspections require the vessel to be taken out of service for a pre-determined amount of time, and often require at least partial removal of the ship's contents to allow access to the areas of interest.

A robust method of evaluating structural health during service would be a great asset to the operation of such a vessel. Structural health monitoring (SHM) would address the difficulties of physical inspection listed above [4]. A typical SHM system involves a discrete vibration source applied discretely to a distinct location while reading the resultant waves some distance away [5]. A difficulty related to this technique is that a

person or device is required to be dedicated as the energy source. Also, SHM can only be performed during specific testing times, usually when the vessel is not in use.

The goal of this study is to identify a technique that would enable real-time SHM in this application. For a system that is capable of monitoring the structural health in real time, a discrete source cannot be realistically used. Therefore, noise can be considered as the energy source. This process is commonly referred to as Diffuse Vibration Interferometry (DVI).

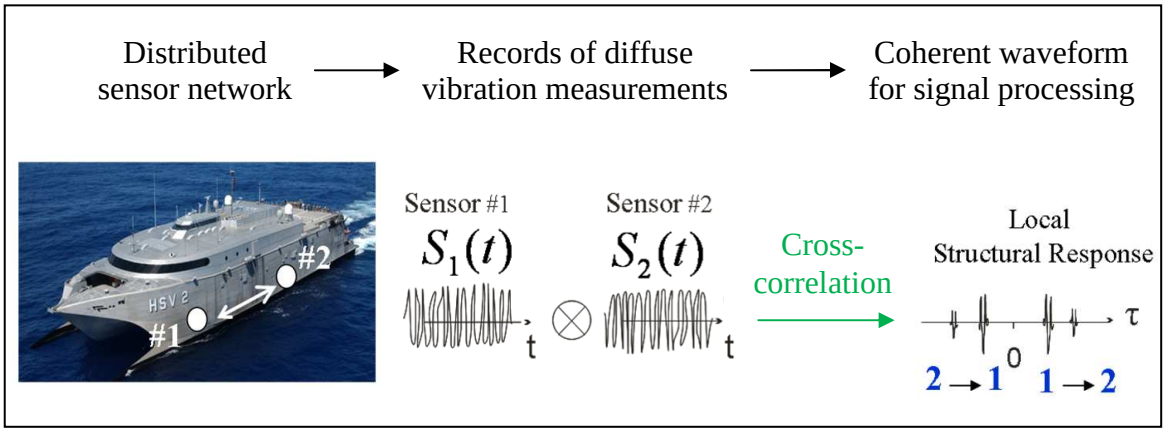

Figure 2: Principle of Diffuse Vibration Inferometry (DVI) for SHM of a naval vessel

Diffuse vibrations, such as those in ambient noise or scattered fields, are often considered to be incoherent and of limited utility. However, there is some coherence between two sensors in a ship that receive vibrations from the same noise sources (e.g. slamming events on the hull) or scatterer (e.g. proud stiffener). The DVI technique resolves the recorded diffuse fields through a correlation process and provides an estimate of the structural impulse response (or Green's function) between a pair of passive sensors (see Figure 2). A coherent waveform emerges once the contributions of the diffuse noise sources traveling through both sensors are accumulated over time. These extracted coherent waveforms are similar to those obtained from conventional measurements between a source and receiver pair, providing a means for SHM without a localized active source, such as a shaker. Therefore, DVI has the potential to expand and improve

SHM system applications since it allows transforming a simple receiver (e.g. strain gage) into a virtual elastic source. This method has been investigated experimentally and theoretically in various environments and frequency ranges: ultrasonics [6-8], structural engineering, [9-10], low-frequency (< 5 kHz) modal properties identification in hydrofoils [11], underwater acoustics [12] and seismology [13-14]. In addition, when implemented with a distributed sensor network, the performance of DVI originates from the high density of cross paths between all pairs of passive sensors which can increase monitoring sensitivity. This study presents DVI analysis results using low frequency random vibration data collected on high-speed vessel HSV2 during sea trials with a wide range of inputs [2]. The resulting coherent waveforms are obtained using DVI from selected strain gages. These coherent waveforms can be used to estimate and monitor the structural response of the ship hull and structural components.

CHAPTER 2: BACKGROUND

Sea trials were performed with the HSV-2 *Swift* near the coast of Norway from May 11 to May 17, 2004. The intent of these trials was to establish safe operating limits for the vessel in a variety of ocean conditions and to gather data to work toward a structural health monitoring system [1]. The trials were run in a variety of sea states (wave conditions), and the vessel was operated throughout a range of speeds at various angles relative to the predominant current direction. Strain gages mounted throughout the ship's structure provided details about the response to a wide variety of external inputs.

2.1 Instrumentation setup

Prior to the test, the ship was outfitted with a network of strain gages. These gages were grouped by the types of measurements they performed: global ("T1"), local ("T2"), and impact response ("T3" and "T4") [1]. The locations of all sensors are documented using HSV-2 *Swift's* schematics, shown in Figure 3 and in Appendix A.

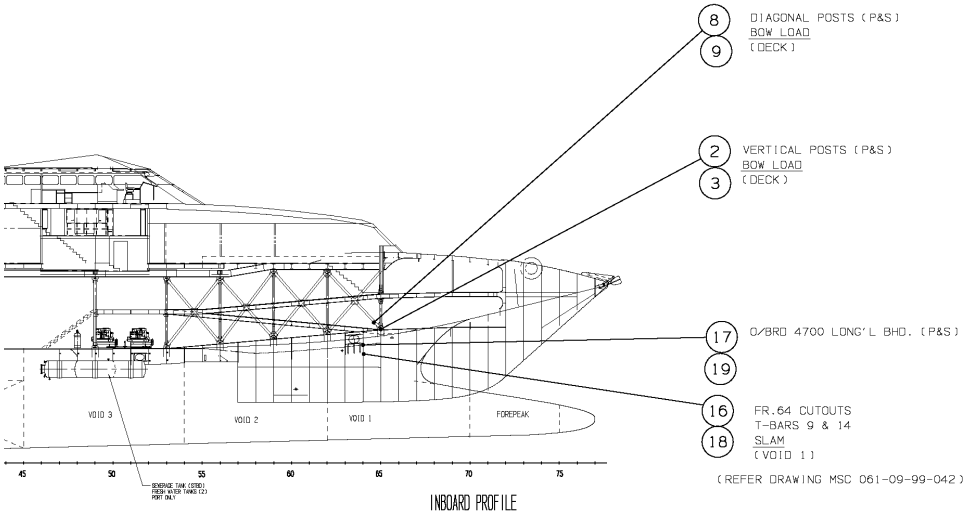

Figure 3: An example schematic of T2 sensor locations [1]

"T1" strain gages were placed on members that were identified as supporting "primary loads," or loads that dictate the sizing of longitudinally or transversely continuous structures. The T1 gages capture the strain level in these members, which can be used to determine the forces imparted into the ship's global structure. There were sixteen T1 gages used in these trials. Descriptions for T1 gage locations are found in Table 5, Appendix A.

Figure 4: Installation of two sensors (T1 and T2) at frame location 26 [1]

"T2" strain gages were located at areas in which significant stress concentrations were anticipated, as determined by finite element analysis (FEA) or by previous experiences of similar vessels. Data from these locations is particularly useful in determining the local stress state of members and can be used in estimating fatigue. Some of the T2 sensor locations were established with multiple gages to capture multi-directional strains. There were twenty-three T2 strain gages producing nineteen T2 sensor locations used in these trials. For descriptions of T2 strain gage placement, see Table 6, Appendix A.

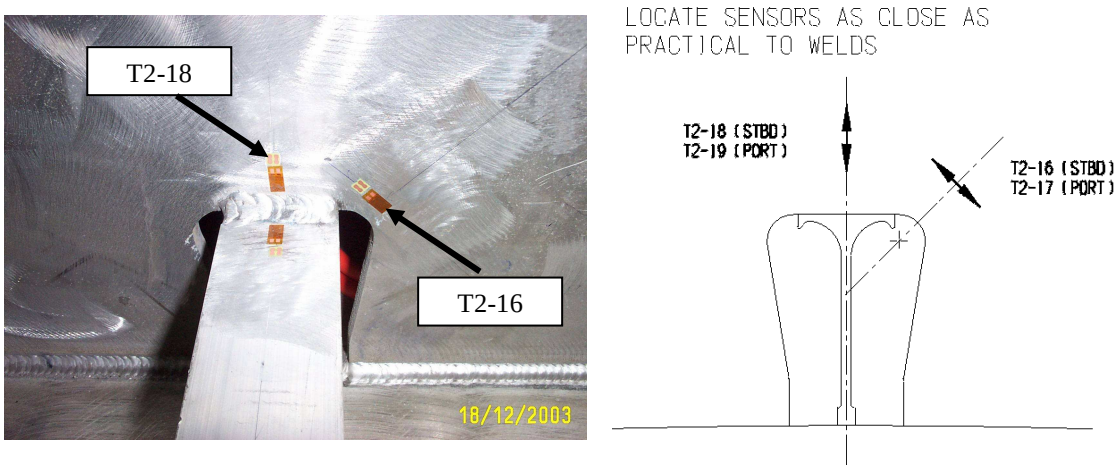

Figure 5: Photograph and schematic detail of sensors T2-16 and T2-18 [1]

"T3" and "T4" strain gages were placed in areas subject to wave impact loading and bow slamming events. They were used to compute uniform static pressure for comparison to design loads. Because the focus of this study is on SHM systems with DVI using ambient energy, as opposed to discrete event inputs, information from these gages was not considered for this research.

Sensors were also included on other areas of the vessel, such as on the launch and recovery ramp, cranes, vehicle and helicopter decks, and gun mounts. Similarly to T3 and T4 gages, the data from these sensors was not used in this study.

The simultaneous output of all sensors was compiled on a central data logging system onboard the vessel. The sampling rate of each sensor's output was 100 Hz, and each test run lasted approximately 30 minutes. This raw strain gage data was the starting point of the processing steps described in Chapter 3.

2.2 Test procedure

The operation plan of the ship during the sea trials was established to collect data at specific speed and heading combinations. Each set of trials was called an “Octagon” due to the pattern of the vessel’s directional course. The ship’s heading was varied in 45° increments relative to the predominant ocean current direction. When eight runs were performed in series with a 45° direction change after each, the resulting path was an octagonal shape.

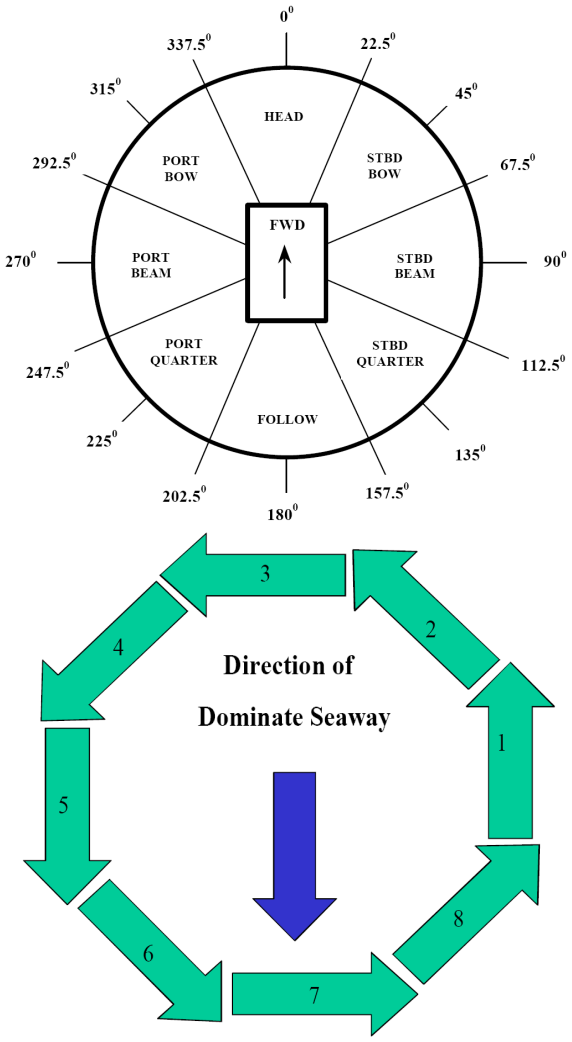

Figure 6: Octagonal maneuver pattern [1]

The height and frequency of the waves encountered during each test was measured at the centerline of the vessel's bow with an on-board over-the-bow wave height system. A secondary wave height measurement was made using a wave buoy positioned inside the area defined by the octagon. The height and frequency of the waves define the "Sea State." See Appendix B for the definition of Sea States 0 – 5. The ship's speed was also varied within pre-determined increments between 2 and 35 knots. The heading and speed were measured by the ship's GPS and gyroscope systems. A summary of the test parameters for each octagon is shown in Table 1.

Table 1: Summary of test ranges

Octagon	Sea State Range	Speed Range (knots)	Headings (Degrees)
1	4-5	2-15	0, 90, 135, 180, 315
2	4-5	2-20	0, 45, 90, 135, 180
3	0-5	2-20	0, 180, 225, 270, 315
4	0-5	2-10	0, 45, 90, 135, 180
5	0-6	2-35	0, 45, 90, 180
6	3-5	2-35	0, 180, 225, 315
7	0-5	2-10	0, 90, 180, 225, 315
8	4-4	20-20	0, 45, 90, 135
9	4-4	2-20	0, 45, 90, 135, 180, 225
10	3-4	2-36	0, 45, 90, 135, 180
11	3-4	2-37	0, 45, 90, 135, 180
12	3-5	2-39	0, 45, 90, 135, 180
13	4-5	2-30	0, 180, 225, 270, 315
14	5-5	2-30	0, 270, 315
15	5-5	2-20	0, 45, 90, 135, 180, 225, 270, 315
16	4-5	2-36	0, 45, 90, 135, 180
17	0-5	2-36	0, 135, 270, 315
18	5-5	2-15	0, 45, 90, 135, 180
19	4-5	2-30	0, 45, 90, 135, 180
20	5-5	2-15	0, 45, 90, 135, 180
21	4-4	2-15	0, 45, 90, 135, 180

CHAPTER 3: DATA PROCESSING

3.1 Data Processing Overview

The data collected during the 2004 Norway trials was stored as raw strain gage recordings over a discrete time interval during ship operation. Figure 7 shows the data recorded from sensor T1-5 from run #182, Octagon 17 on May 16, 2004, with a speed of 35 knots, a 270° heading relative to the dominate seaway, and a level 5 sea state. Sensor T1-5 is located in the port side keel between the engine and fuel tank.

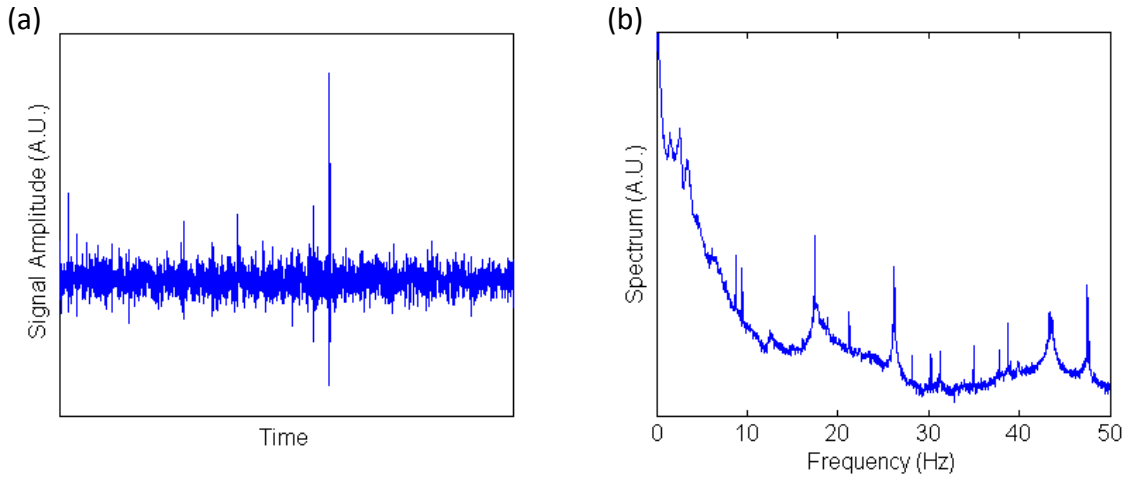

Figure 7: T1-5 Sensor data in the time domain (a) and frequency domain (b)

The discontinuous peaks seen in the data when viewed in the time domain (Figure 7(a)) are associated with slamming inputs into the ship's hull. When considering the frequency spectrum (Figure 7(b)), the vibrations at low frequencies (less than 12 Hz) are likely generated by the interactions of waves and the ship's hull and sea loadings. In contrast, the multiple spectral peaks in the region of frequencies greater than 15 Hz suggests that this range is dominated by vibrations from rotating machinery with multiple nodes.

Prior to computing the cross-correlations to generate the coherent waveform for signal processing, the amplitude spectrum of the continuous vibrations recordings was analyzed

in order to assess the influence of the vibration origin on the DVI technique. Furthermore, the DVI technique works best when the random vibrations are uniform in space and time. Hence the effects of high amplitude slam events (as seen in Figure 7(a)) should be minimized in the signals from the strain gages since they might otherwise dominate the time delay of the cross-correlation function. To do so, the continuous vibration recordings were first homogenized using the procedure illustrated in Figure 8.

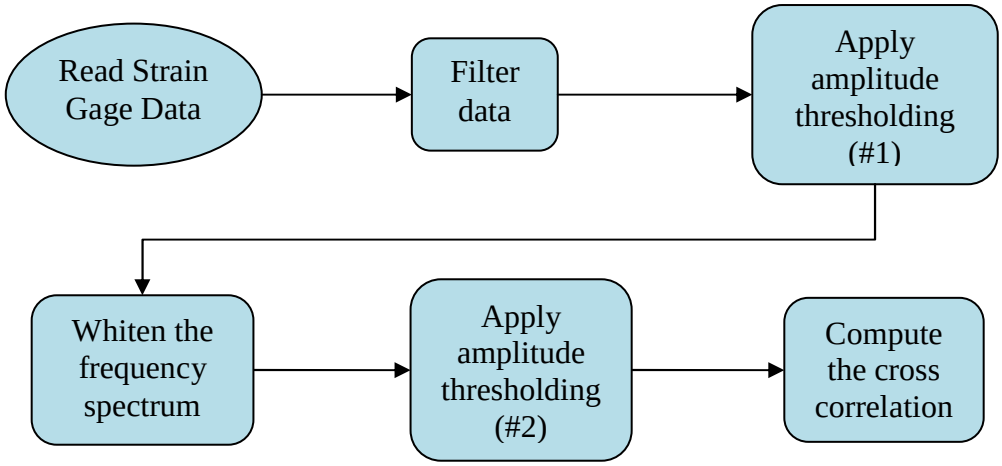

Figure 8: Flowchart of Processing Sequence

The influence of this processing sequence was investigated with a parametric study using a variety of values to alter the effects of each step. In this manner, the relative contribution of each step could be ascertained. The results of each processing step are shown in Figures 9-15. Sensor T1-6 from Octagon #9 is used in Figures 10-15 to illustrate each step.

3.2 Pre-Processing Steps

Read Strain Gage Data

The raw strain gage output was collected and stored as individual channels. Figure 9 shows the data from all 35 T1 and T2 channels collected during the execution of Octagon #9.

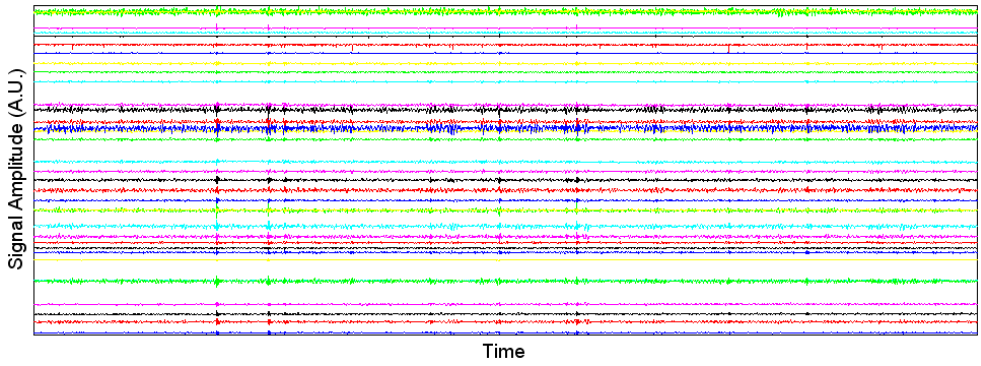

Figure 9: Unprocessed data from all T1 and T2 sensors

The data for sensor T1-6 is shown in Figure 10. This shows the signal amplitude and frequency content in the time domain, as well as the frequency amplitude in the frequency domain.

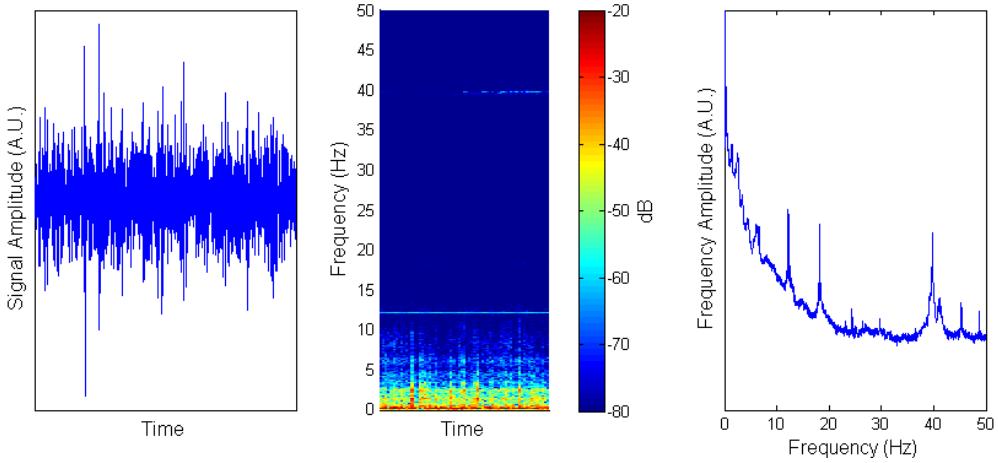

Figure 10: Unprocessed data from sensor T1-6

Filtering the data

The data was filtered by fitting its amplitude spectrum to a Hanning window. This was done to reduce the occurrences of sensor measurement irregularities. The Hanning function is defined as

$$w(n) = 0.62 - 0.48\left|\frac{n}{N} - 0.5\right| + 0.38\cos\left(2\pi\left(\frac{n}{N} - 0.5\right)\right)$$

where $0 \leq n \leq N$, and N=window length-1 [15].

A Hanning window (the area containing the Hanning function's curve) is depicted graphically in Figure 11.

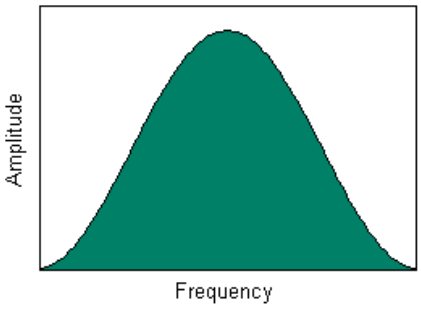

Figure 11: An example of a Hanning window

The frequency range that defines the x-axis of the Hanning window is a predetermined parameter. The frequency range was a focus of the data processing experimentation described in Section 4.4.

The result of applying a Hanning window to the data is depicted in Figure 12.

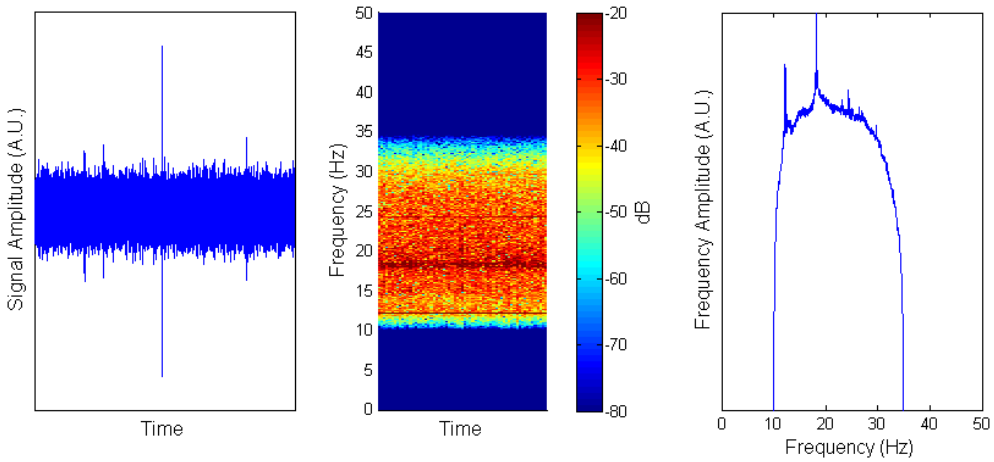

Figure 12: T1-6 data with Hanning filter applied

Apply amplitude thresholding (#1)

Amplitude thresholding was then applied by truncating the signal at a pre-determined value above and below zero. This was performed to reduce the influence of "slamming" events, such as large waves contacting the ship's hull. The threshold value was varied in the experimentation discussed in Section 4.3.

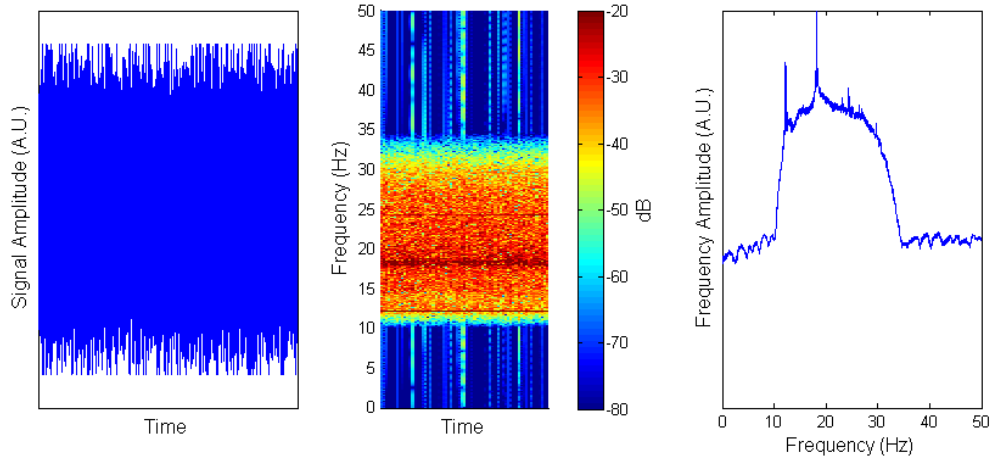

Figure 13: T1-6 data with first amplitude thresholding applied

Whiten the frequency spectrum

The frequency spectrum was whitened after the amplitude thresholding. Because the sources in this study are by nature variable and not discrete and predictable values, the whitening was performed to reduce the effects of changes in these sources.

Whitening was performed by

$$F(\varpi) = \frac{P(\omega)}{|P(\omega)| + \varepsilon} \cdot w(n)$$

where P(ω) is the Fourier transform of the input signal, ε is a Wiener filter constant, and $w(n)$ is the Hanning window (defined previously). The Wiener filter constant is implemented to reduce noise content present in the signal by comparison with a constant value that is a multiple of the standard deviation of the data set. The actual value for the multiplier was the subject of a portion of the experimentation discussed in Chapter 4.

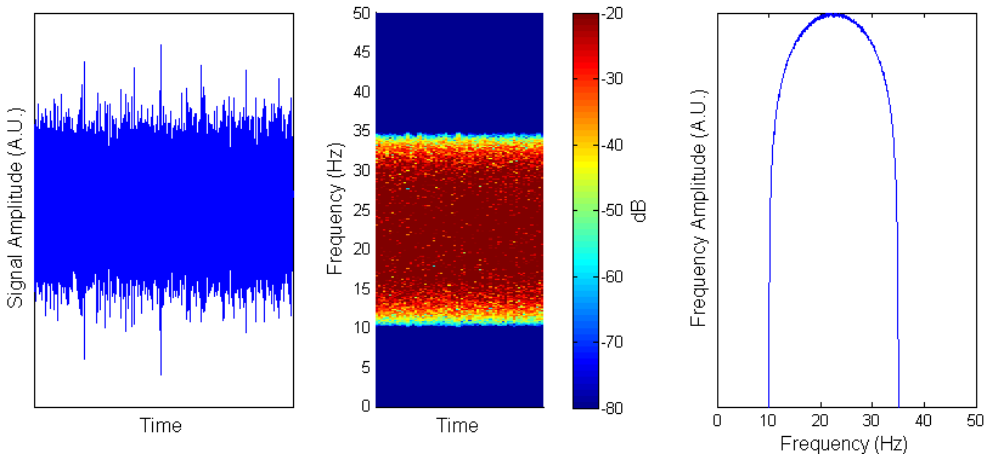

Figure 14: T1-6 data after frequency whitening

Apply second amplitude thresholding

Amplitude thresholding was applied to the whitened data to avoid distortion of the FFT calculation, leading to amplifications of artificial broadband peaks in the time-domain data. This was done similarly to the first amplitude thresholding, truncating data outside of the pre-determined band.

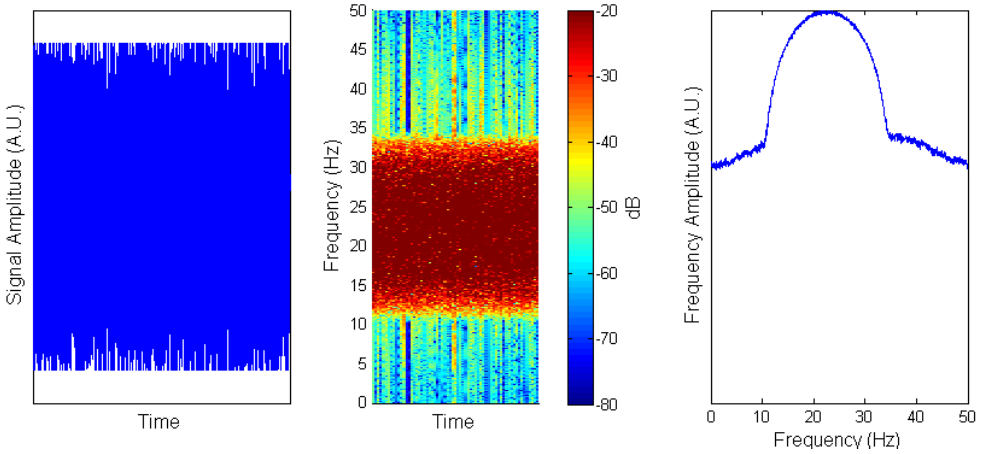

Figure 15: T1-6 data with second amplitude thresholding applied

3.3 Computing the cross-correlation

The cross-correlation was then computed with the processed data. Before computing the cross-correlation, the sensor pairs needed to be established. With 35 T1 and T2 sensors, there are 595 possible pair combinations.

The existence of diffuse vibrations in the ship's structure ensures that all propagation paths between any two passive sensors are fully illuminated. The expected value of the temporal cross-correlation function between two sensors, $C_{12}(t)$, can be computed from the diffuse field $S_1(t)$ measured by sensor #1, and the diffuse field $S_2(t)$ measured by sensor #2, after integration over the observation period *T*:

$$C_{12}(t) = \int_0^T S_1(\tau) S_2(\tau + t) d\tau$$

For the sensor pairs' two signals x and z with i time data entries, the time-discretized version of the cross-correlation is defined as

$$C_k^{<S_1,S_2>} = \sum_i S_{1i} \cdot S_{2i+k}$$

where k is the time shift of signal S_2. The cross-correlation values $C_k^{<S_1,S_2>}$ are compiled into the array $\underline{C}^{<S_1,S_2>}$ [16].

The cross-correlation is maximized when the product of S_{1i} and S_{2i+k} is at a maximum. This occurs when k is adjusted such that S_{2i+k} most closely matches S_{1i} in both amplitude and phase.

An example of the result of a cross-correlation calculation is shown in Figure 16.

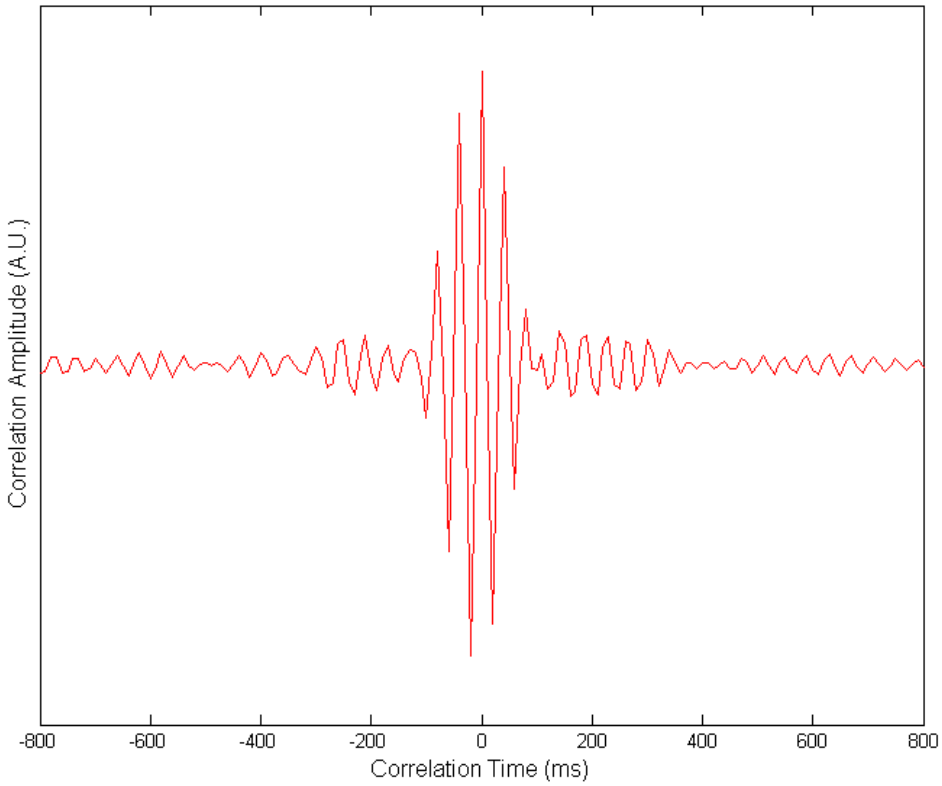

Figure 16: Cross-Correlation between Sensors T1-6 and T1-7

The energy measured by each sensor can be considered to exist in the form of either a standing wave or a travelling wave. In the case of a travelling wave, the time at which the cross-correlation is at the highest magnitude is considered to be the "arrival time" of the estimated impulse response. Alternatively, when considering the system's energy to exhibit standing wave characteristics with mode shapes, the peak cross correlation represents the phase delay between the two data sets.

CHAPTER 4: PARAMETRIC STUDY OF THE DVI PROCESS

While the process used for data reduction was outlined in Chapter 3, the particular parameter values used by the data pre-processing procedure needed to be established. This chapter reviews the process used to determine the optimal parameters for data processing.

4.1 Parametric study

The data processing procedure and parameters were evaluated by varying the process outlined in Section 3.1. Some of the steps were omitted, and the values of some of the variables were changed. Table 2 lists the parameters and ranges of values used in the processing experimentation.

Table 2: Parameter values used in experimentation

Parameters	Values
Amplitude Thresholding #1	on / off
Threshold #1 STD	1-10
Whitening	on / off
Wiener filter constant	0-20
Amplitude Thresholding #2	on / off
Threshold #2 STD	1-10
Frequency Window	multiple, between 1 and 45 Hz

The amplitude thresholdings were performed by truncating all values greater than the specified number of standard deviations away from zero. Higher "STD" values result in a larger range of data to be passed through the thresholding steps without modification.

The Wiener filter constant was varied within the range shown. It was implemented as a multiplier to the standard deviation of the data set. A value of zero would eliminate the Wiener filter, while a higher value would increase the effect of the Wiener filter.

The frequency window is the range over which the Hanning window is created during the data filtering step. The frequencies in the middle of the range are enhanced, while those outside of the range are diminished.

4.2 Criteria

A method was needed to evaluate and compare the contribution of each of the variables discussed in Section 4.1.1. Two criteria were identified as appropriate indicators for each processing scenario: the peak value of the normalized cross-correlation and the "Peak-to-Fluctuation Ratio."

The normalized cross-correlation was defined as:

$$\text{Normalized Cross-Correlation} = \frac{\sum_{runs} C_{S_1 S_2}}{\sqrt{\sum_{runs} Energy_{S_1}} \cdot \sqrt{\sum_{runs} Energy_{S_2}}}$$

where $C_{S_1 S_2}$ is the cross-correlation of the signals between sensors S_1 and S_2, and $Energy_{S_1}$ and $Energy_{S_2}$ are the integrals of the two sensors' signals. Each term is summed across every run in a given octagon set. By definition, the normalized cross-

correlation is a term between 0 and 1. A higher value indicates a higher normalized cross-correlation.

The "Peak-to-Fluctuation Ratio" (PFR) is defined as the maximum normalized cross-correlation value divided by the standard deviation of the normalized cross-correlation for time lags larger than one second away from the peak time delay, as calculated from the cross correlation. A higher PFR indicates a stronger correlation term at the main arrival as compared with areas away from the main arrival.

A graphical illustration of the PFR is found in Figure 17. In it, the PFR is represented as

$$PFR = \frac{x}{y}$$

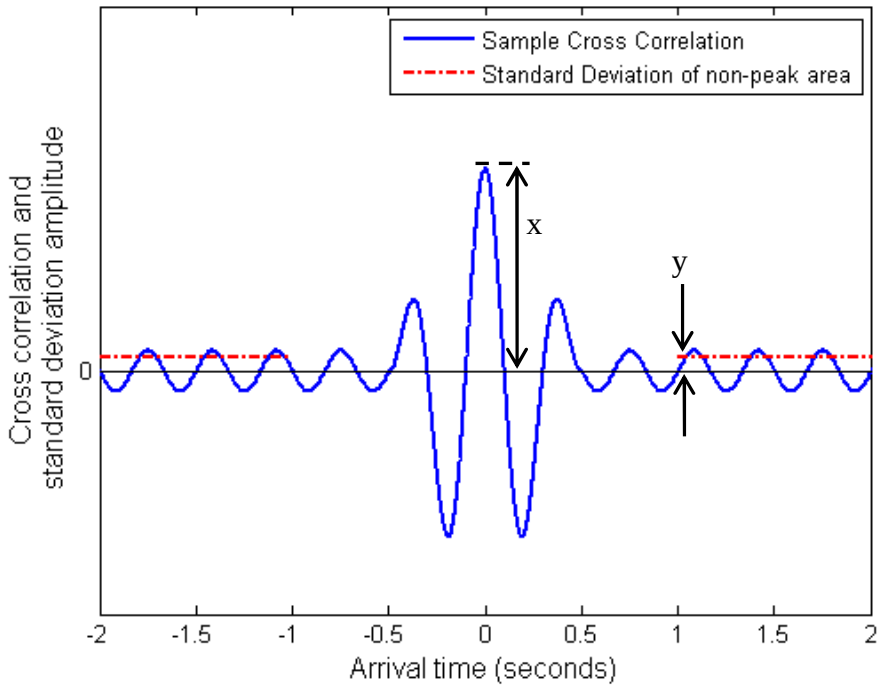

Figure 17: Illustration of Peak-to-Fluctuation Ratio

4.3 Amplitude Thresholding and Whitening Experimentation

A matrix of variables for the processing parameters was established (see Table 3). It was created by altering one or two parameters within the ranges listed in Table 2 for each processing scenario. A set of parameters was assumed for "Scenario #1". The parameter values in subsequent scenarios that differ from those in Scenario #1 are highlighted in green.

Table 3: Scenario processing log

	Amplitude Thresholding #1		Whitening		Amplitude Thresholding #2		Frequency
	on / off	Threshold STD	on / off	Wiener filter STD	on / off	Threshold STD	Window
Scenario #1	on	3	on	0	on	2	15-35
Scenario #2	on	1	on	0	on	2	15-35
Scenario #3	on	2	on	0	on	2	15-35
Scenario #4	on	5	on	0	on	2	15-35
Scenario #5	on	8	on	0	on	2	15-35
Scenario #6	on	10	on	0	on	2	15-35
Scenario #7	off		on	0	on	2	15-35
Scenario #8	on	3	on	1	on	2	15-35
Scenario #9	on	3	on	3	on	2	15-35
Scenario #10	on	3	on	6	on	2	15-35
Scenario #11	on	3	on	8	on	2	15-35
Scenario #12	on	3	on	10	on	2	15-35
Scenario #13	on	3	off		on	2	15-35
Scenario #14	on	3	on	0	on	1	15-35
Scenario #15	on	3	on	0	on	4	15-35
Scenario #16	on	3	on	0	on	6	15-35
Scenario #17	on	3	on	0	on	8	15-35
Scenario #18	on	3	on	0	on	10	15-35
Scenario #19	on	3	on	0	off		15-35
Scenario #20	on	3	on	0	on	2	1-12
Scenario #21	on	1	on	0	on	2	1-12
Scenario #22	on	10	on	0	on	2	1-12
Scenario #23	off		on	0	on	2	1-12
Scenario #24	on	3	off		on	2	1-12
Scenario #25	on	3	on	3	on	2	1-12
Scenario #26	on	3	on	10	on	2	1-12
Scenario #27	on	3	on	0	off		1-12
Scenario #28	on	3	on	0	on	1	1-12
Scenario #29	on	3	on	0	on	10	1-12
Scenario #30	on	1	on	0	off		15-35
Scenario #31	on	5	on	0	off		15-35
Scenario #32	on	10	on	0	off		15-35
Scenario #33	on	20	on	0	off		15-35

To expedite evaluation, three representative tests (Octagons 15, 18, and 19) and four sensor pairs (5+7, 8+10, 7+13, and 10+13) were considered during each processing scenario. The values for the normalized cross-correlation and the PFR defined in Section 4.1.2 were found for each Scenario by octagon and sensor pair.

Plots of the maximum normalized cross-correlation for the octagons considered and two of the sensor pairs (T1-5+T1-7 and T1-8+T1-10) for each scenario are shown in Figure 18.

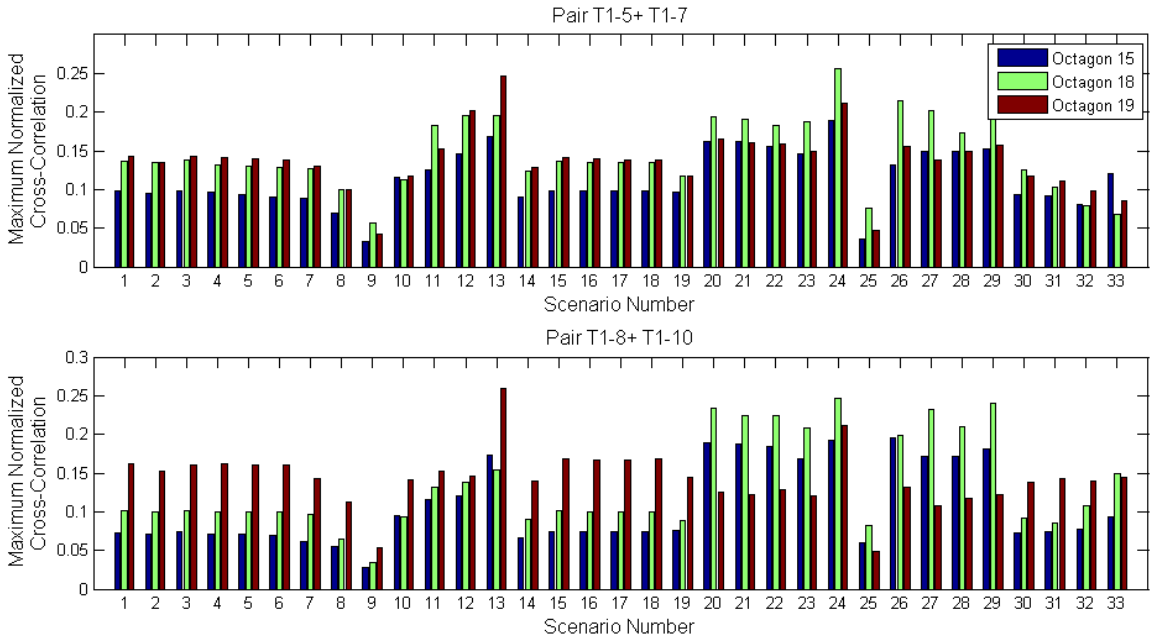

Figure 18: Plot of Maximum normalized cross-correlation values for each scenario evaluated

A plot of the PFR values for each scenario and the same octagons and sensor pairs used in Figure 18 is shown in Figure 19.

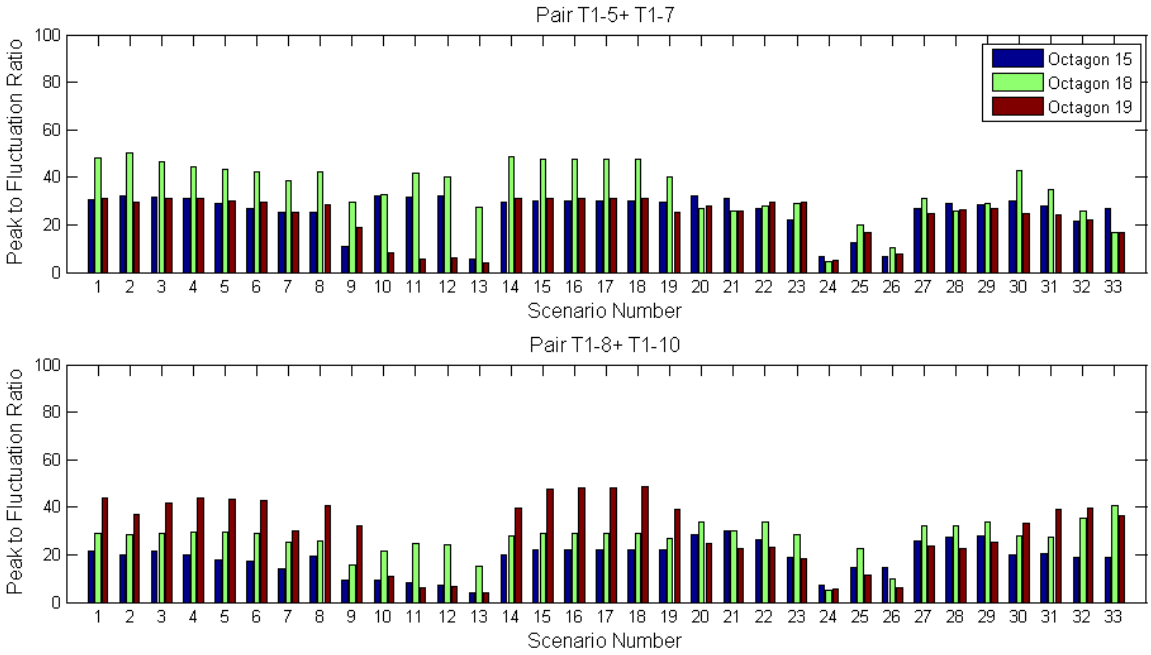

Figure 19: Plot of PFR values for each scenario evaluated

Scenarios 13 and 24, which had no frequency whitening step after the first amplitude thresholding, produced the highest normalized cross-correlation for all octagons. However, the lack of frequency whitening also resulted in a low PFR, meaning the actual main arrival value was not significantly distinguishable from the correlation values away from the arrival.

When a non-zero Wiener filter was implemented during the frequency whitening (as in Scenarios 8 – 12, 25, and 26), effects were seen in both the normalized cross-correlation and PFR metrics. Wiener filter STDs above 6 resulted in a higher peak normalized cross-correlation, while values below 6 decreased the peak normalized cross-correlation. For all scenarios in which a Wiener filter was used, the PFR was reduced as compared to scenarios in which there was no Wiener filter used.

The effects of changing the values of the amplitude thresholding proved to be minimal. Within the range of threshold values used (1 through 10) the effects on normalized cross-correlation and PFR were very small. When the thresholding was turned off altogether (as in Scenarios 7, 18, 23, and 27) a decrease in the normalized cross-correlation and PFR metrics from 12-18% was noted.

The results from varying the amplitude thresholding and the frequency whitening were similar between the two frequency windows considered. Scenarios 1-19 were filtered at 15-35 Hz with either the first amplitude thresholding, the whitening, or the second amplitude thresholding varied. Scenarios 20-29 were similarly created by making changes to one of the three sets of variables, but were filtered from 1-12 Hz. The results of changing each variable had a similar effect for both groups of frequency ranges.

With consideration to each variable's influence on both the normalized cross-correlation and PFR, it was apparent that frequency whitening should be employed without a Wiener filter. It was also evident that including both amplitude thresholding steps was beneficial, but the result was not especially sensitive to the specific values of the selected thresholding STDs. This result is a favorable indication for the proposed processing strategy's use in SHM systems, since it yields a DVI system that is not overly sensitive to particular input parameters.

4.4 Frequency Band Experimentation

There are multiple sources of the energy that propagate through the structure of vessels such as the HSV-2 *Swift*. They include waves contacting the ship's hull, the operation of the propulsion engines, operation of other machinery onboard, and also the movement of the ship's occupants. Figure 20 shows the unprocessed frequency content of two sensors, one near the stern (T1-1) and one 55 meters closer to the bow (T1-7).

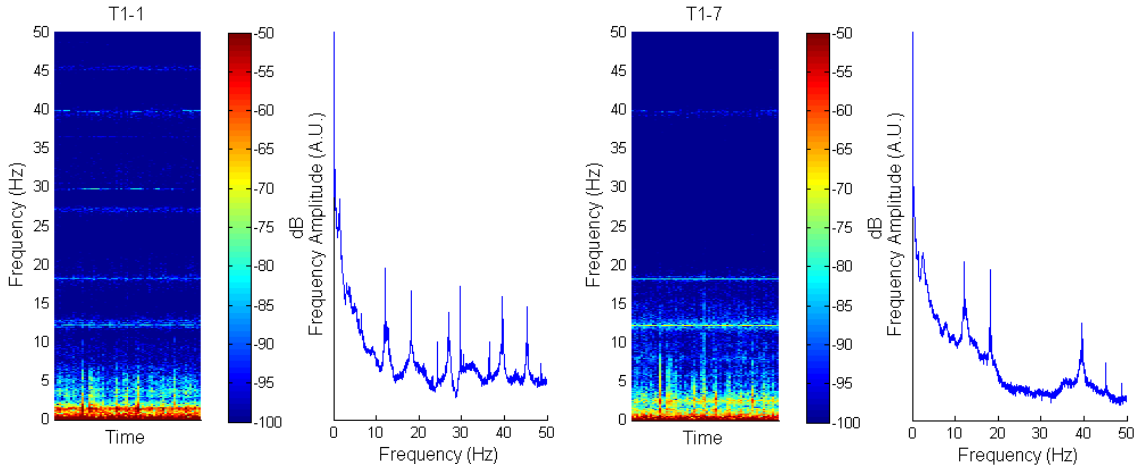

Figure 20: Frequency content of two sensors (T1-1 and T1-7) in Octagon #9

The frequency range that is used to define the Hanning window in the filtering stage can affect the results of the processing. The sensors' signals will be enhanced within the center of the chosen range, where the peak of the Hanning curve is located, and will be diminished in areas outside of the chosen range.

Several ranges of frequencies were identified for evaluation. The ranges used were chosen in 10 Hz and 20 Hz bands. The performance of each frequency range was evaluated by plotting the normalized cross-correlation term as defined in Chapter 3.

Figure 21 shows the normalized cross-correlation plots for sensor pair T1-5+T1-7 during Octagon #9.

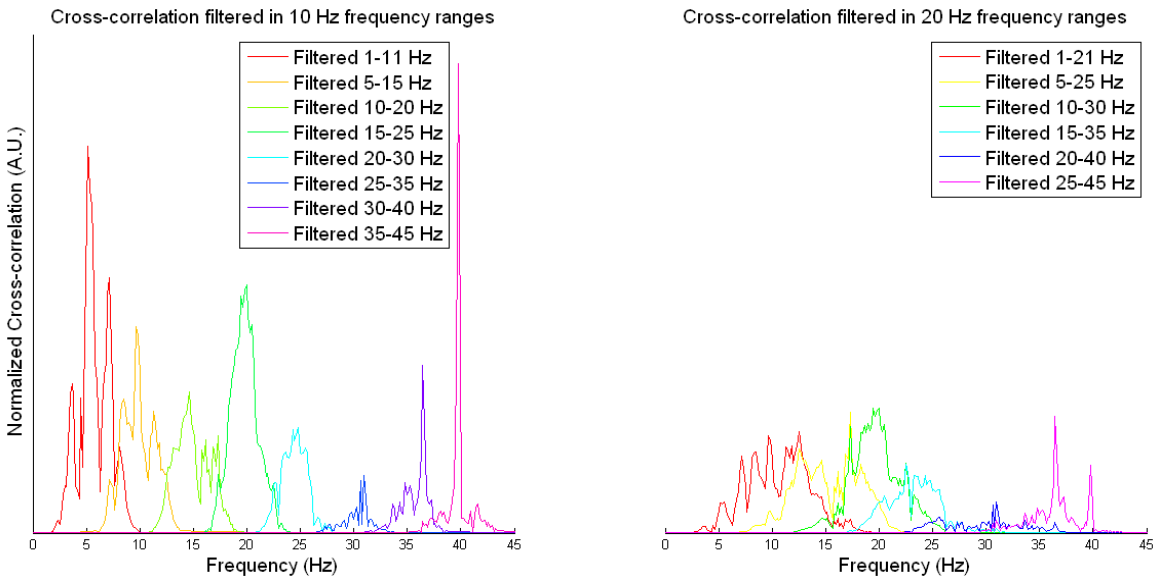

Figure 21: Amplitude spectrum of the normalized cross-correlation for various frequency processing bands, sensor pair T1-10+T1-13, Octagon #9

In general, the higher frequency ranges have less energy than the lower ones, evident from the relative magnitudes of the normalized cross-correlation terms. There is an exception around 40 Hz, at which frequency there is a relative peak in the amount of energy present. The goal of this study is to achieve the most uniform correlation result possible. This would be represented by a normalized cross-correlation curve displaying an amplitude distribution as similar as possible to the initial Hanning window used for data frequency whitening, with minimal discontinuities.

The cross-correlation waveforms for sensor pair T1-10+T1-13, Octagon #9 are shown in Figure 22.

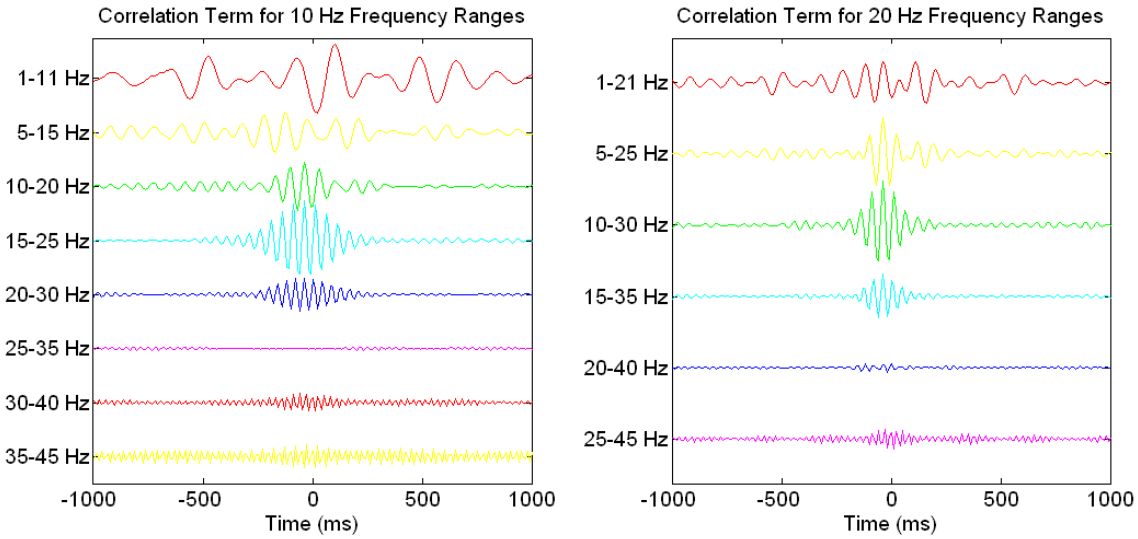

Figure 22: Correlation term for frequency processing bands, sensor pair T1-10+T1-13, Octagon #9

The shapes and amplitudes of the correlation terms can be compared for the different filter ranges. Some filter ranges, such as 1-11 Hz and 1-21 Hz, have arrival waveforms that are indistinct and spread out, indicating a poor correlation. Others, such as 25-35 Hz and 20-40 Hz, have relatively low amplitudes, meaning the amplitude of the cross-correlation waveform is low. For a wave-based monitoring system, selecting the frequency ranges associated with the most distinct arrivals is preferred when computing the cross-correlation waveforms.

To determine the preferred frequency range for processing, both the shape of the normalized cross-correlation in the frequency domain and the time delay waveform of the correlation term in the time domain were considered. The band judged as most likely to provide a distinct and repeatable correlation result was the frequency range between 15 and 35 Hz.

4.5 Summary of parametric value experimentation results

After consideration of the results of the experimentations, the parameter values shown in Table 4 were chosen as most conducive to SHM applications for the HSV-2 *Swift*:

Table 4: Variable values chosen for processing

Variables	Values
Amplitude Thresholding #1	on
Threshold #1 STD	3
Whitening	on
Wiener filter constant	0
Amplitude Thresholding #2	on
Threshold #2 STD	3
Frequency Window (Hz)	15-35

Processing was run for all sensors and octagons with the values listed in Table 4. Cross-correlation was performed on all sensor pairs. The results, as they apply to SHM in the HSV-2 *Swift*, are presented in Chapter 5.

CHAPTER 5: APPLICATION

5.1 Pair combinations for cross-correlation

Stable cross-correlation results are a requirement for a viable SHM system. Without a consistent and repeatable cross-correlation, it would be impossible to detect true change in a structure as opposed to measurement and calculation variation. A measure of stability of the cross-correlation is a comparison of the time at which the peak cross-correlation occurs for a variety of tests. The performance of the DVI technique was systematically investigated for selected pairs of T1 strain gages identified in Figure 23. Each sensor shown is located in the keels of the ship. T1-5, T1-6, and T1-7 are located on the port side, while T1-8, T1-9, and T1-10 are located on the starboard side directly opposite the ship's centerline.

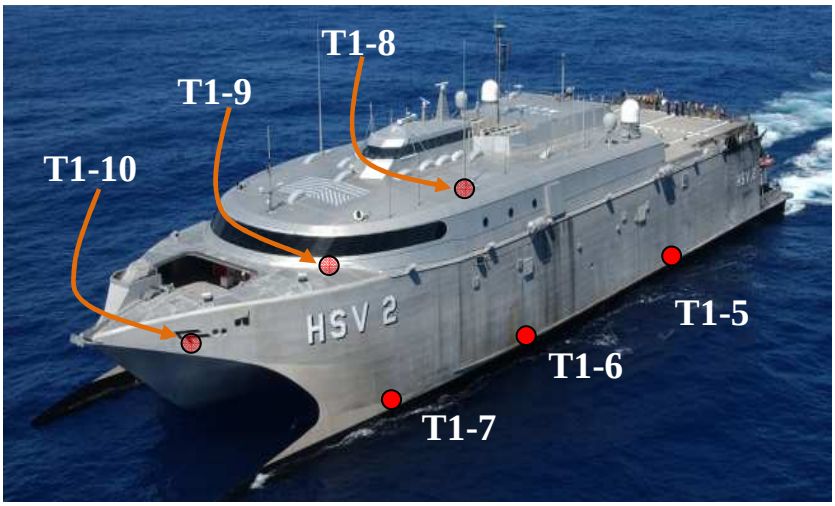

Figure 23: Three port side (T1-5 – T1-7) and three starboard side (T1-8 – T1-10) sensors on HSV 2 – *Swift*

Figure 24 (a) – (f) shows the evolution of the cross-correlation waveforms over the 21 Octagons for six combinations of the sensors identified in Figure 23. The peaks of each correlation waveform are indicated by red dots. Figure 24 (g) and (h) show the time

value of each of the waveform peaks versus the octagon count. The divisions between the seven days of sea trials are indicated by black bars in Figure 24 (a) – (f) and by dashed vertical lines in Figure 24 (g) and (h).

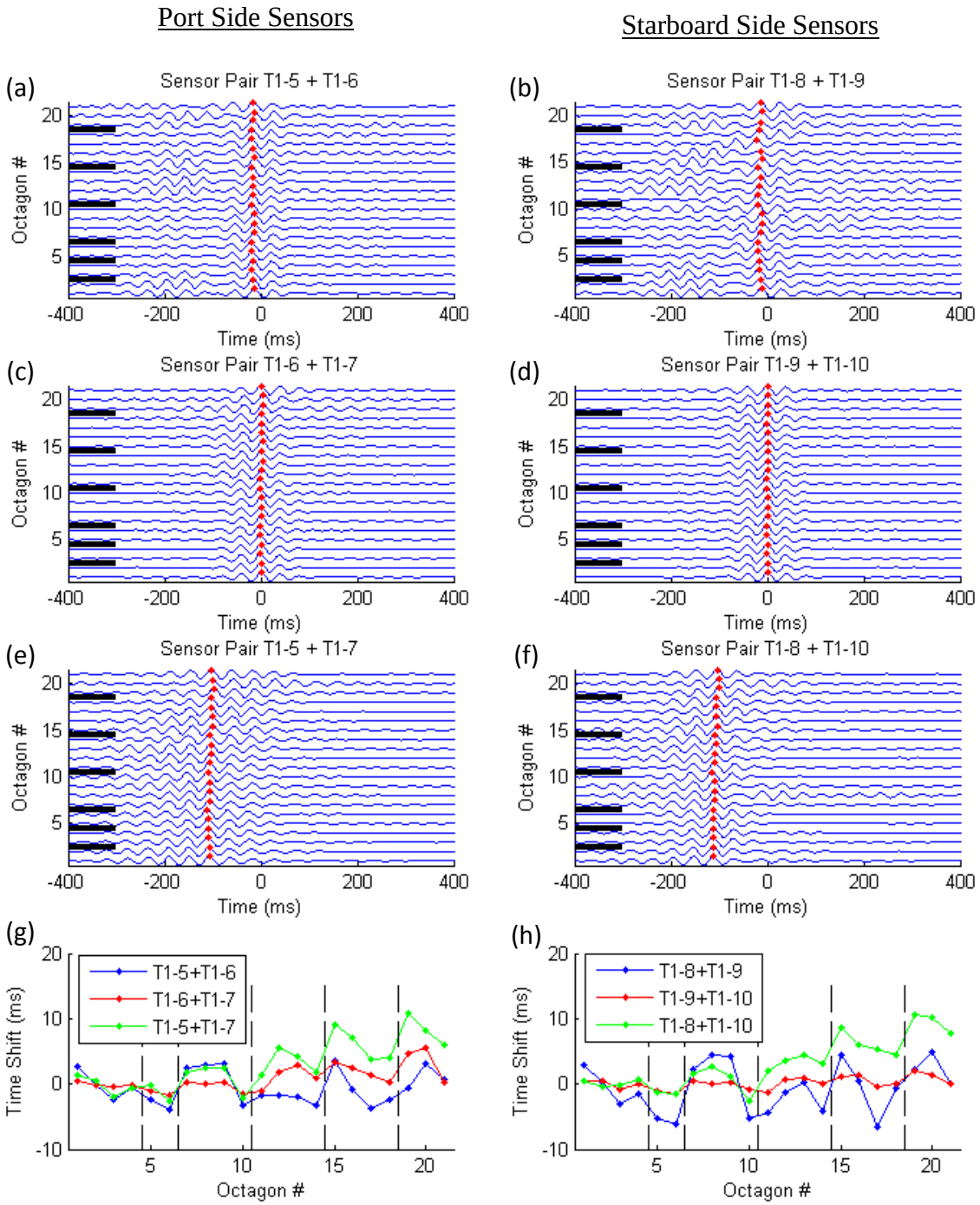

Figure 24: Cross-correlation waveforms for all octagons for six sensor pairs ((a) – (f)). Shifts in peak arrival time by octagon for each sensor pair ((g) – (h)).

Because there were no significant structural changes during the trials and the test duration was relatively short, low fluctuation in cross-correlation is expected for a stable, consistent system. The maximum time shift along the 21 Octagons is for the six sensor pairs shown is 11 ms, occurring in sensor pair T1-8+T1-10 (starboard side keel). These small, but consistent, structural variations on the port and starboard keels are likely induced by fuel level variations or expansions and contractions of the ship's structure due to temperature changes throughout the testing period. The low fluctuation in this system's cross-correlations indicates that the proposed processing steps are a viable solution to SHM in this application.

5.2 Monitoring web of sensors for a SHM system

When implemented with a distributed sensor network, the results of implementing DVI principles are improved with a high density of connecting paths between all sensor pairs. With 35 total T1 and T2 sensors available, there are 595 possible pair combinations for cross-correlation analysis. Figure 25 illustrates a "Monitoring Web" of sensors which can be created by using the top 40%, or 254, sensor pairs (as determined by the normalized cross-correlation). This monitoring web could potentially be integrated in a SHM system to assist the crew of HSV-2 *Swift* in operation decisions.

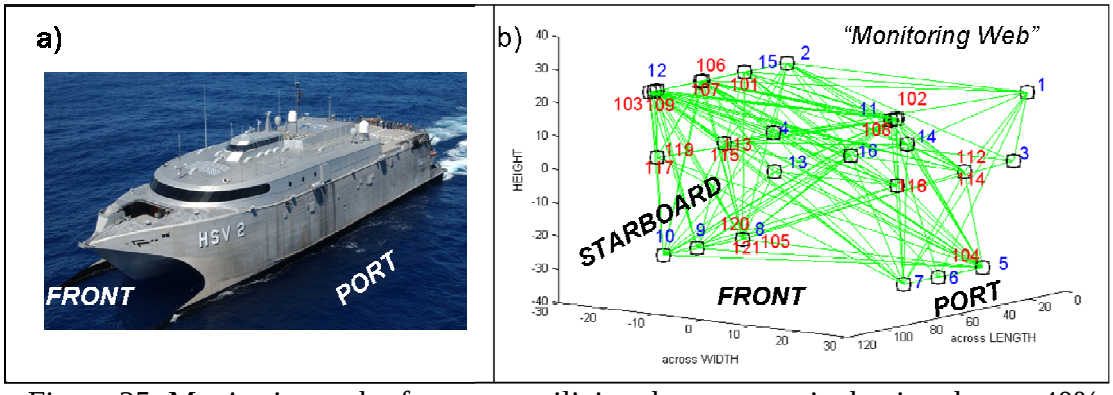

Figure 25: Monitoring web of sensors, utilizing the sensor pairs having the top 40% cross-correlation values

The time delays for each sensor pair were computed using the cross-correlation method discussed previously. The longitudinal distance between sensors was plotted versus the time delays (averaged across all octagons) in Figure 26.

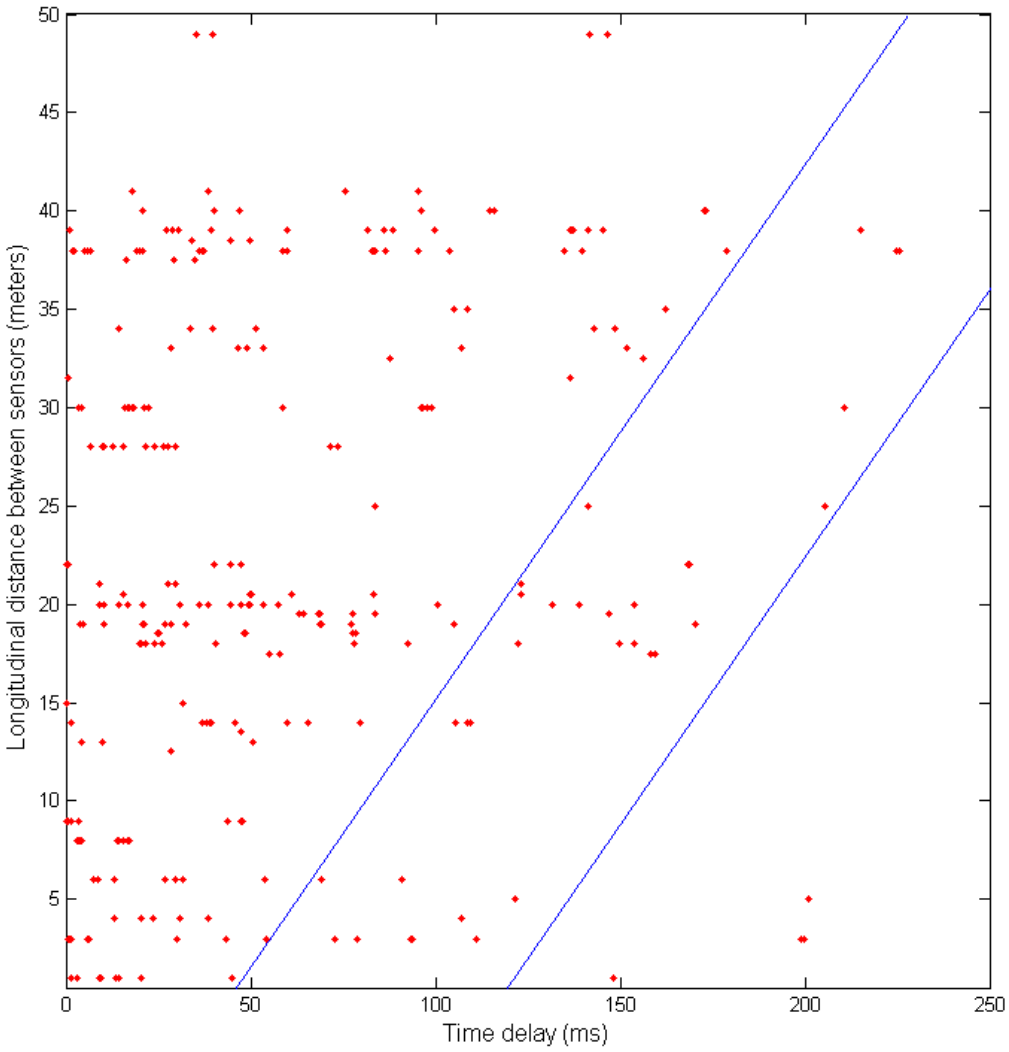

Figure 26: Longitudinal distance between sensor pairs vs. time delay

A proportional relationship between time delay and sensor separation distance is desirable for practical SHM applications. High resolution in time delay offset yields a more robust system for real-time monitoring of structures. As evident from Figure 26, not all sensor pairs exhibit such a proportional relationship. This could be the result of

several factors. The true distance between the sensor pairs may differ from the longitudinal distance when there is a significant vertical or lateral distance between the sensors, or if the wave propagation path between the sensors is indirect, as is frequently experienced on a naval vessel. Also, the particular area of the vessel spanned by a given sensor pair could experience a discrete energy content discontinuity if a local energy source is present in that area.

A group of sensor pairs demonstrating roughly proportional time delays to separation distances was selected for further analysis. These pairs are displayed in Figure 26 within the area defined by the blue lines. Figure 27 shows the correlation term waveforms of the sensor pairs identified within the window referenced in Figure 26.

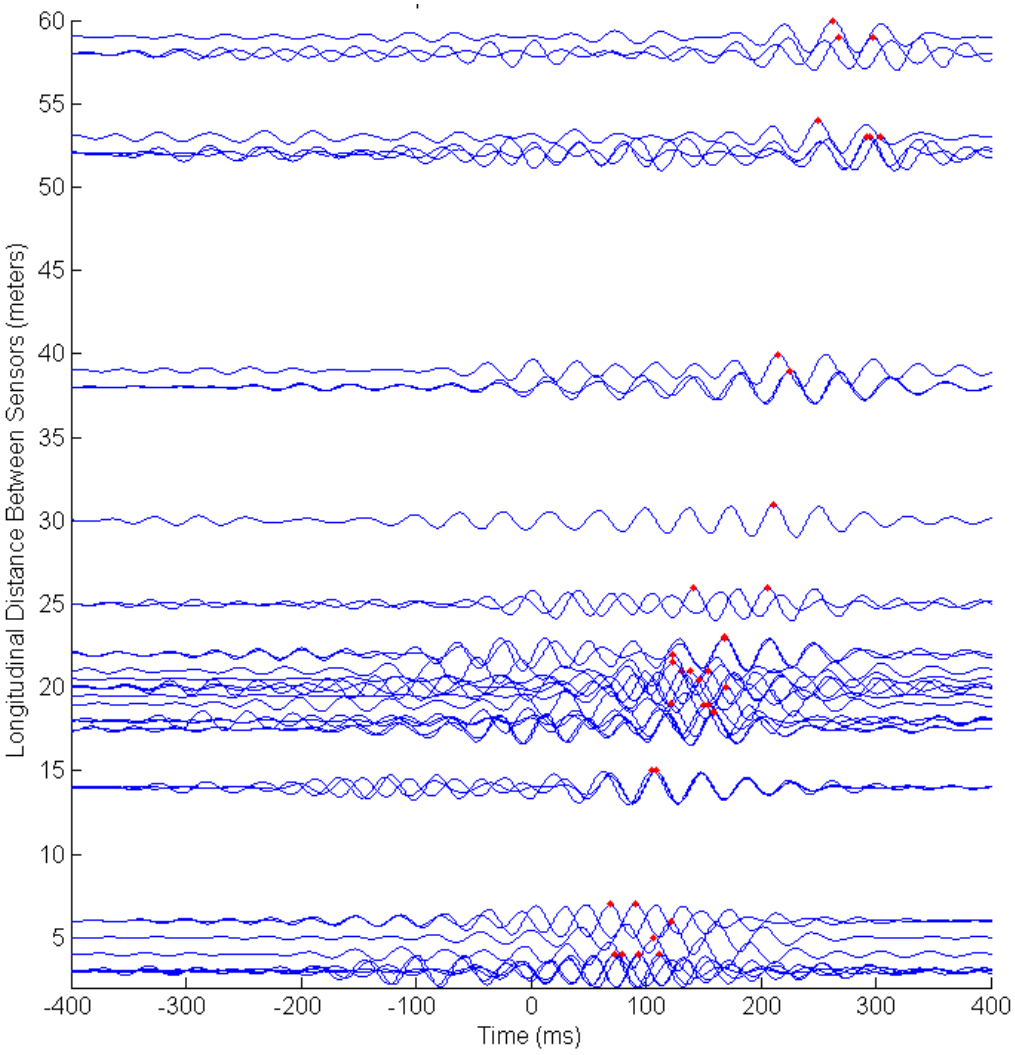

Figure 27: Correlation waveform plots for various sensor separation distances

The nature of the coherent waveform shown by peak cross-correlation time for increasing separation distance of the selected sensor pairs illustrates a potentially viable SHM system.

CHAPTER 6: CONCLUSIONS

The preceding chapters illustrated that the processing method employed in this study is viable for producing waveforms useful for passive structural health monitoring. Whether the energy is assumed to exist in the form of propagating waves or in mode shapes, there exists a structural signature of the HSV-2 *Swift* that can be used for structural health monitoring. The cross-correlation time delay offsets for each sensor pair had little variation between the different groups of tests performed over a period of seven days. A stable, repeatable peak cross-correlation time offset will allow for discernment of a change in this value due to structural change in the vessel.

The processing is not especially sensitive to the actual values of amplitude thresholding or whitening terms. The values presented in Chapter 4 were judged to yield slightly better correlation terms than the alternatives within the range evaluated, but a considerable difference is not expected when using other values for the thresholding or whitening terms. This lack of sensitivity to chosen values is favorable for DVI, as the parameter values chosen for processing are not likely to artificially influence the cross-correlation results.

Unlike the choice in thresholding and whitening variables, the frequency band used during the data filtering can significantly affect the DVI results. The signal amplitude in the sensors showed areas of discontinuous peaks at certain frequencies due to the amount of energy present at those frequencies. Some frequency ranges did not produce a usably distinct cross-correlation waveform, making the identification of a distinct time delay value difficult. Effort was taken to ensure the range selected had the most uniform frequency content and that there was sufficient energy to produce a reasonable correlation.

An optimal result of a DVI study is that the cross-correlation time delay would be proportional to separation distance for every sensor pair. However, this does not

consistently apply to the real-world case examined here. Some pairs do not exhibit such a relationship. This can be a result of inaccurate estimation of the separation distance, a discontinuity in energy content between the sensors, or many other factors. In contrast, some sensor pairs do display a proportional relationship between cross-correlation time delay time and separation distance, as illustrated in Figure 27. Selection of sensor pairs exhibiting such a relationship can lead to accurate predictions of the vessel's structural health.

CHAPTER 7: RECOMMENDATIONS

The nature of the HSV-2 Norway trials was one of limited duration, lasting only seven days, with no significant events imparting critical damage to the ship's structure. The true effectiveness of the data processing and sensor monitoring steps presented in this report is best demonstrated over a long service interval. Similarly, if a known defect or structural compromise was introduced into the ship's structure, the degree of change in the correlation time delay would indicate the effectiveness of this processing methodology.

An unknown aspect in establishing the relationship between sensor distance and cross-correlation waveform time delay is the actual distance separating sensor pairs. Longitudinal dimensions of each sensor were provided, but vertical and lateral spacing was unknown. Better estimates of the sensor separation distances could be made with this information. The length of the actual wave propagation path, along the structures connecting the sensors, would be a further refinement to increase this value's accuracy.

APPENDIX A
SENSOR LAYOUT

Appendix A contains descriptions and illustrations of the locations of the sensors referenced in this report. All figures and tables in this section were published by Brady et al [1].

Table 5: Summary of T1 global response strain gage channels

No.	Measurement Location			Load	Details
T1-1	Bracket, Fr 6	Port	Deck	PCM	Vertical or horizontal direction, On bracket side, close to curved edge
T1-2	Bracket, Fr 6	Stdb	Deck	PCM	"
T1-3	B/head, Fr 12	Port	Anteroom	Combination	Vertical direction, 500mm off floor, close to rider
T1-4	B/head, Fr 12	Stbd	Anteroom	Combination	"
T1-5	Keel, Fr 26	Port	Void 6	Bending	On longitudinal vertical keel. One quarter of frame span, approximately 300 mm from bulkhead or frame on lower section of web
T1-6	Keel, Fr 46	Port	Void 3	Bending	"
T1-7	Keel, Fr 61	Port	Void 2	Bending	"
T1-8	Keel, Fr 26	Stbd	Void 6	Bending	"
T1-9	Keel, Fr 46	Stbd	Void 3	Bending	"
T1-10	Keel, Fr 61	Stbd	Void 2	Bending	"
T1-11	Foredeck cutout, Fr 67	Port	Foredeck	PCM	Aft corners of cutout on insert plate, transverse direction
T1-12	Foredeck cutout, Fr 67	Stbd	Foredeck	PCM	"
T1-13	Web, Fr 65	Centerline	Void 2	Split	6000mm off centerline, upper section of web, transverse direction
T1-14	Web, Fr 6	Centerline	J/room	Split	1170mm off centerline, lower section of web, transverse direction
T1-15	Crossbrace, Fr 25	Stbd	Deckhead	PCM	300mm along aluminum box beam member from Batwing. The Batwing is a joint detail that connects the aluminum crossbraces above the Mission Deck with the portal structure, see Figure 14. This complements the measurement T2-1, see Table 11.
T1-16	Web, Fr 31	Centerline	Void 5	Split	Lower section of web, transverse direction

Table 6: Summary of T2 stress concentration measurements

No.	Measurement Location			Load	Details
1	Crossbrace, Fr 25	Stbd	Deckhead	PCM	End of Batwing, adjacent T1-15
2	Fwd steel post, Fr 65	Port	Deck	Bow load	Axial on member, lower section
3	Fwd steel post, Fr 65	Stbd	Deck	Bow load	"
4	Keel, Fr 26	Port	Void 6	Bending	Adjacent keel web/frame join
5	Keel, Fr 26	Stbd	Void 6	Bending	"
6	Side door aft top corner	Stbd	Deck	Combination	Top corner of hatch opening aligned 45 deg across corners
7	Side door fwd top corner	Stbd	Deck	Combination	"
8	Fwd steel diagonal, Fr 64	Port	Deck	Bow Load	Axial, resolve with T2-2 for total load.
9	Fwd steel diagonal, Fr 64	Stbd	Deck	Bow load	Axial, resolve with T2-3 for total load.
12	Deck joiner doubler, Fr 34	Port	Void 5	parking load	Adjacent doubler weld, beneath deck, for stress concentration
13	Deck joiner doubler, Fr 34	Stbd	Void 5	parking load	"
14	Deck skin, Fr 34	Port	Void 5	parking load	Lower mission deck skin, midspan for nominal stress, near T2-12
15	Deck skin, Fr 34	Stbd	Void 5	parking load	"
16	Tbar #9 cutout, Fr 64	Port	Void 1	slam	On frame web, adjacent to cutout. Tbars numbered outboard from 4700 long.
17	Tbar #9 cutout, Fr 64	Stbd	Void 1	slam	"
18	Tbar #14 cutout, Fr 64	Port	Void 1	slam	"
19	Tbar #14 cutout, Fr 64	Stbd	Void 1	slam	"
20	Tbar end connection keel, Fr 26	Stbd	Void 6	sea pressure	Measures Tbar end strain outboard of T2-5
21	Tbar end connection portal, fr 26	Stbd	Void 6	sea pressure	Measures Tbar local response component below mission deck level on outboard shell structure

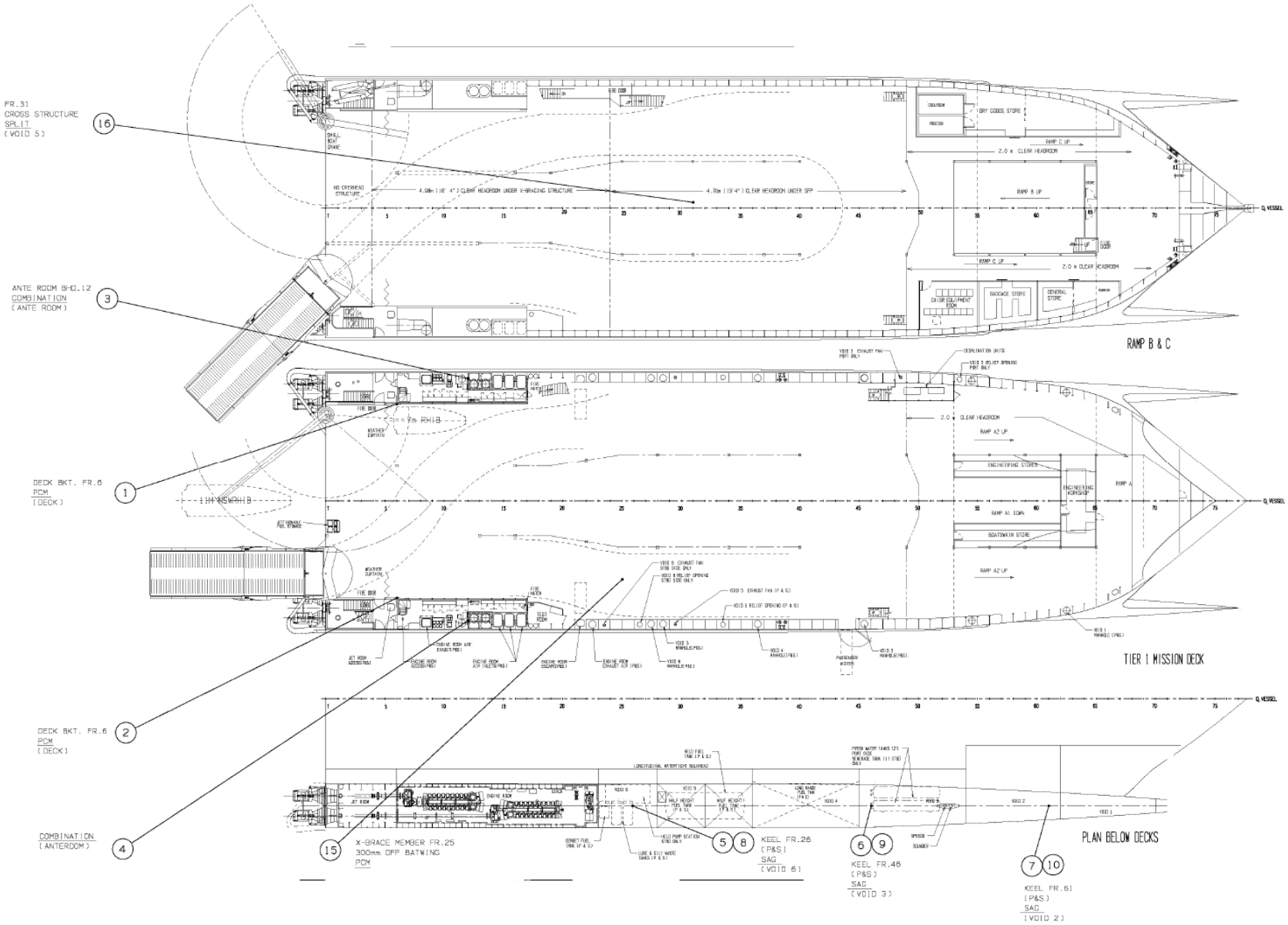

Figure 28: Layout of T1 sensors (view #1)

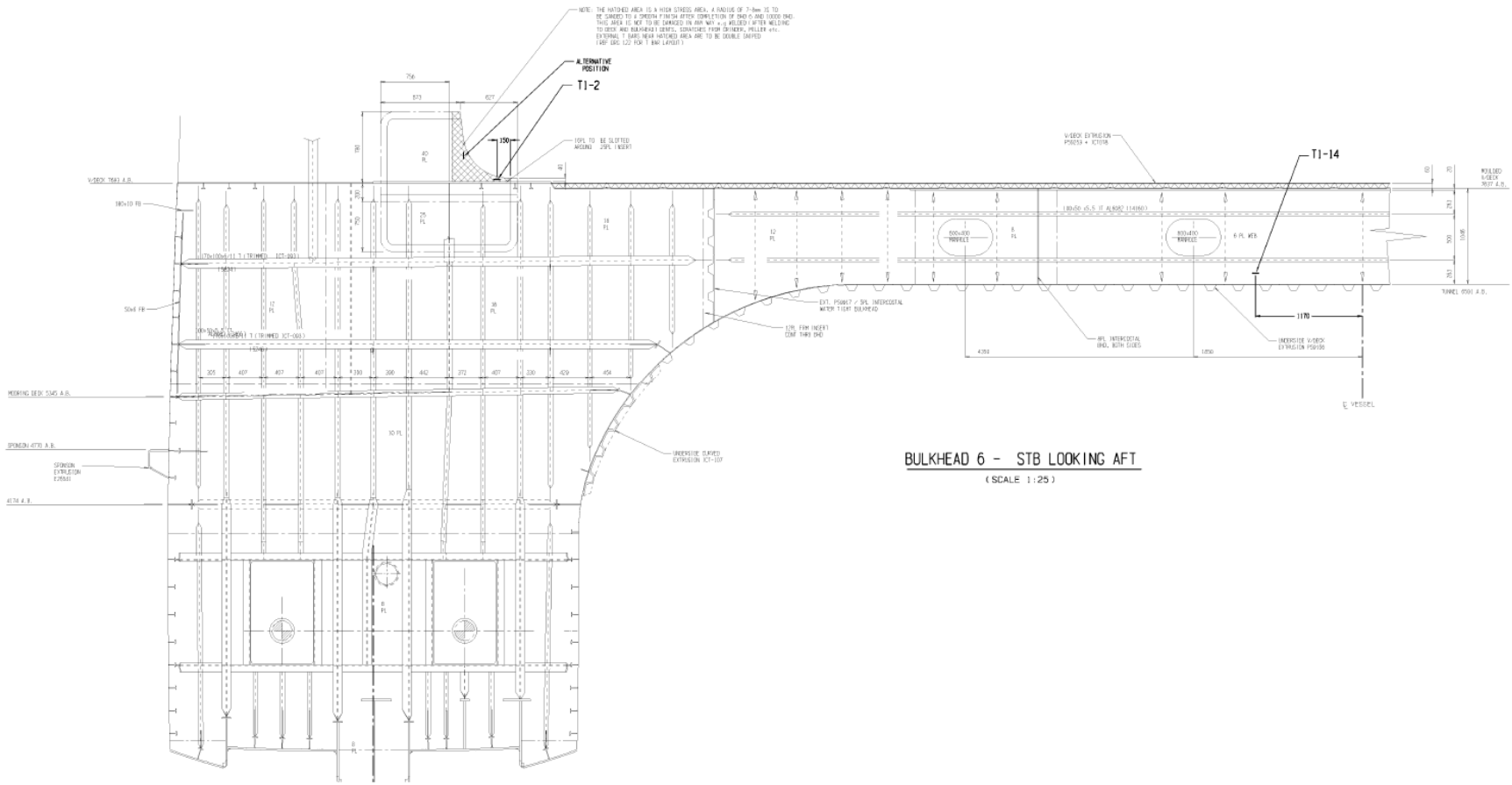

Figure 29: Layout of T1 sensors (view #2)

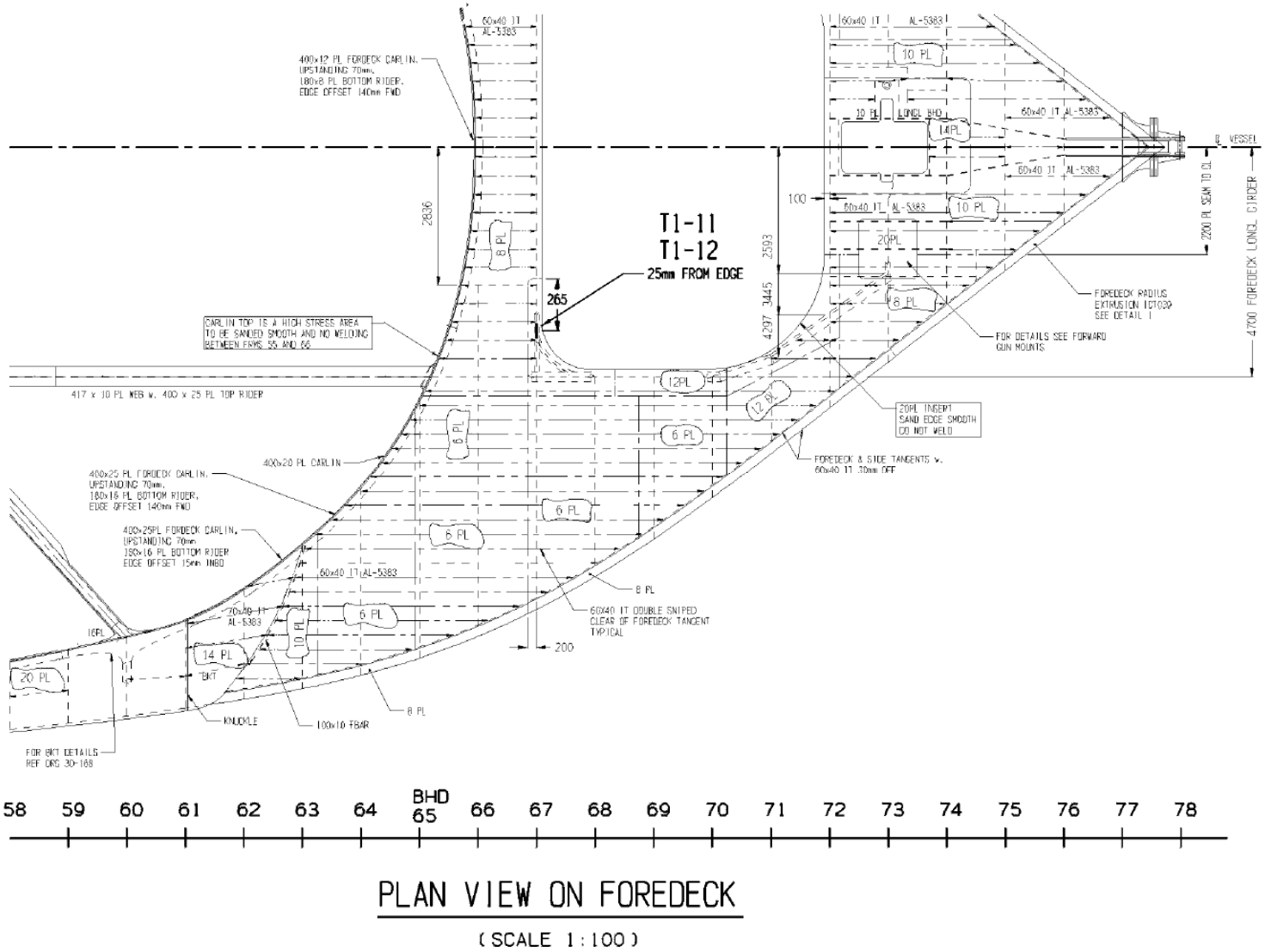

PLAN VIEW ON FOREDECK

(SCALE 1 : 100)

Figure 30: Layout of T1 sensors (view #3)

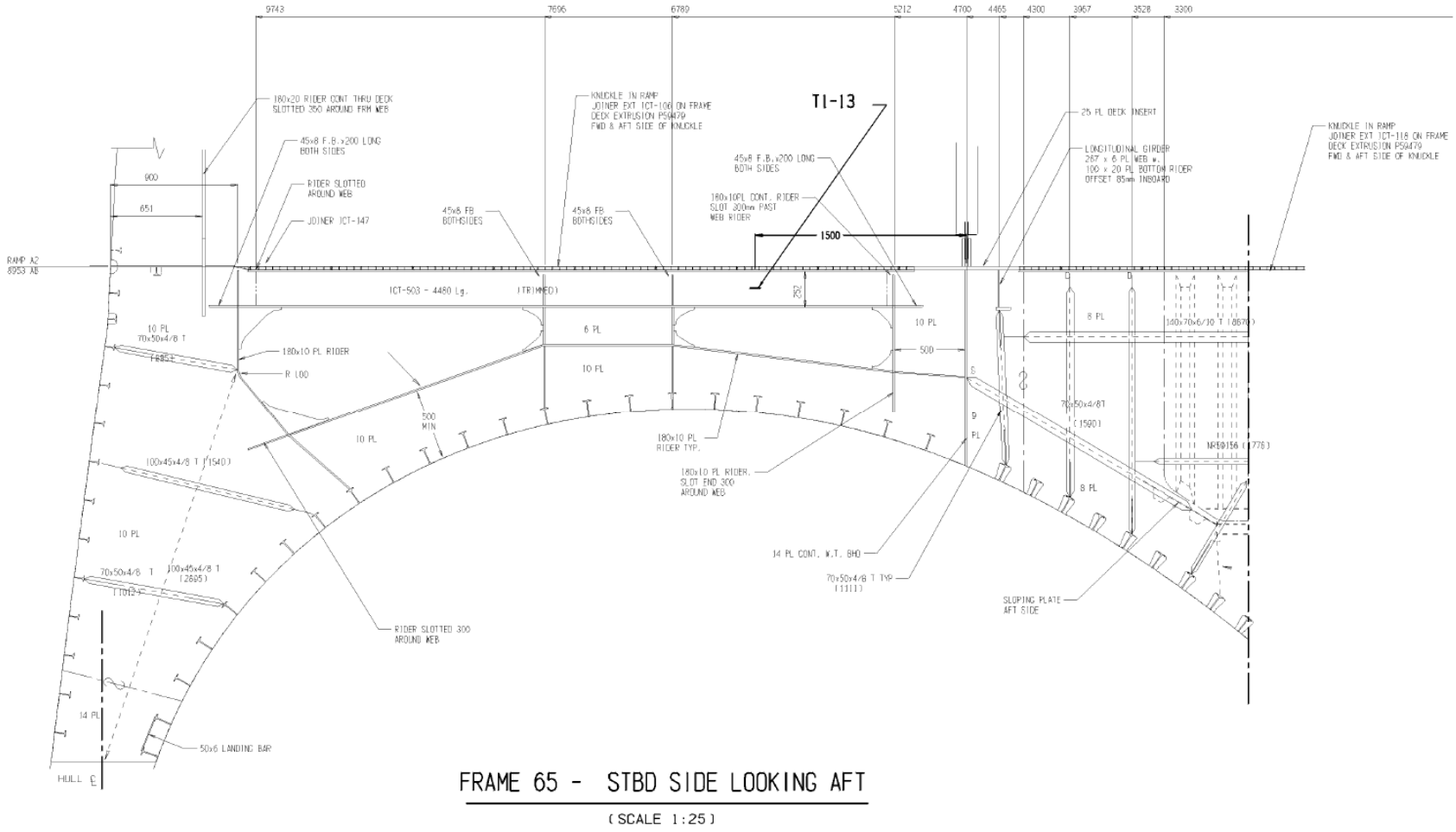

Figure 31: Layout of T1 sensors (view #4)

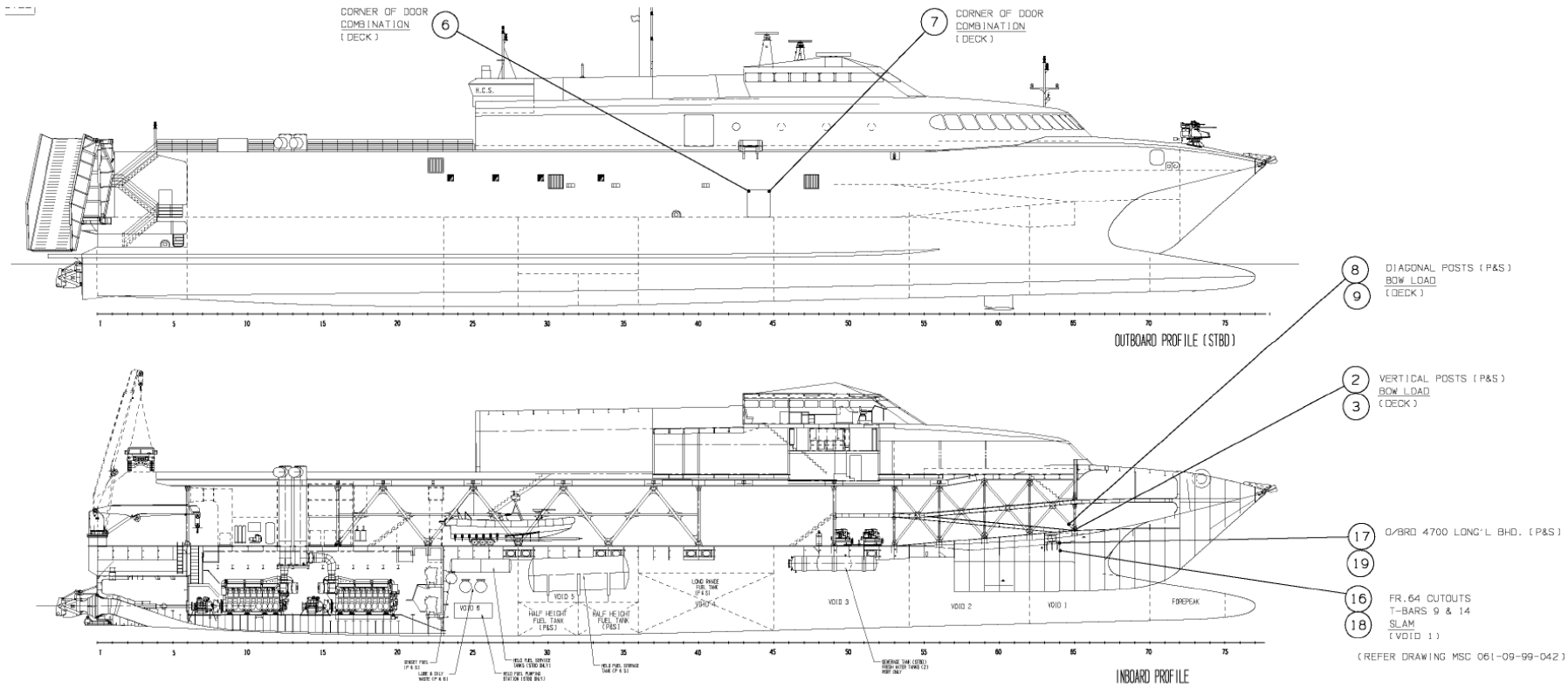

Figure 32: Layout of T2 sensors (view #1)

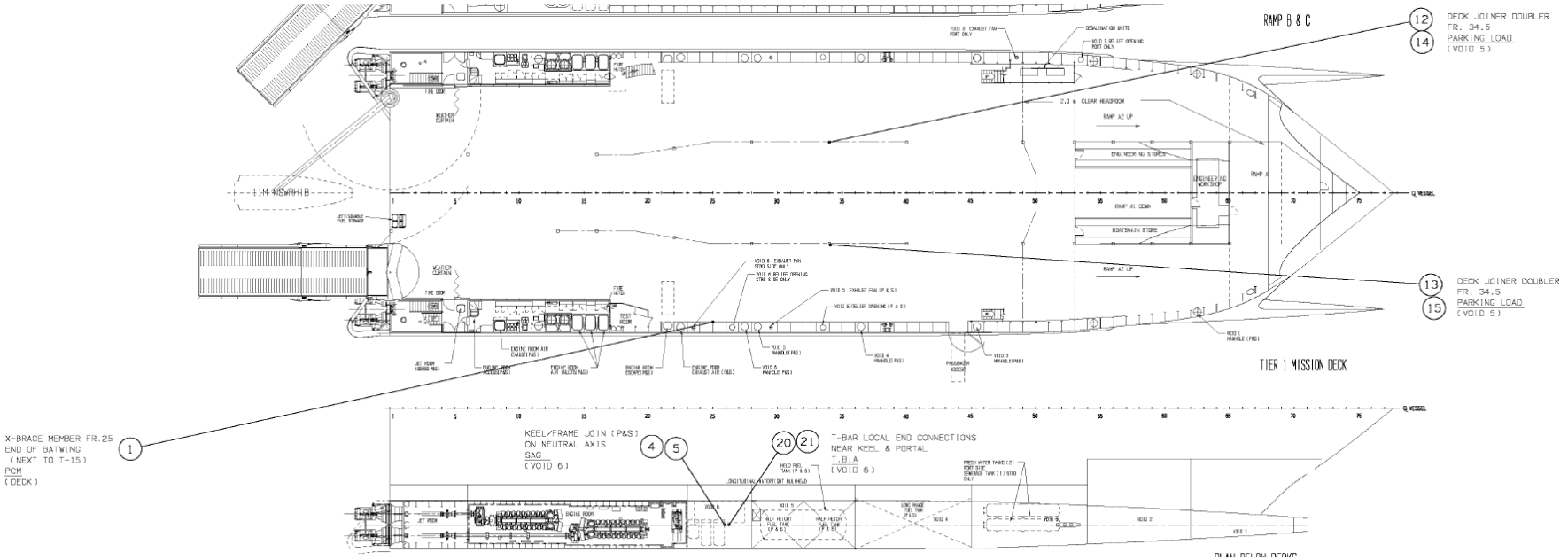

Figure 33: Layout of T2 sensors (view #2)

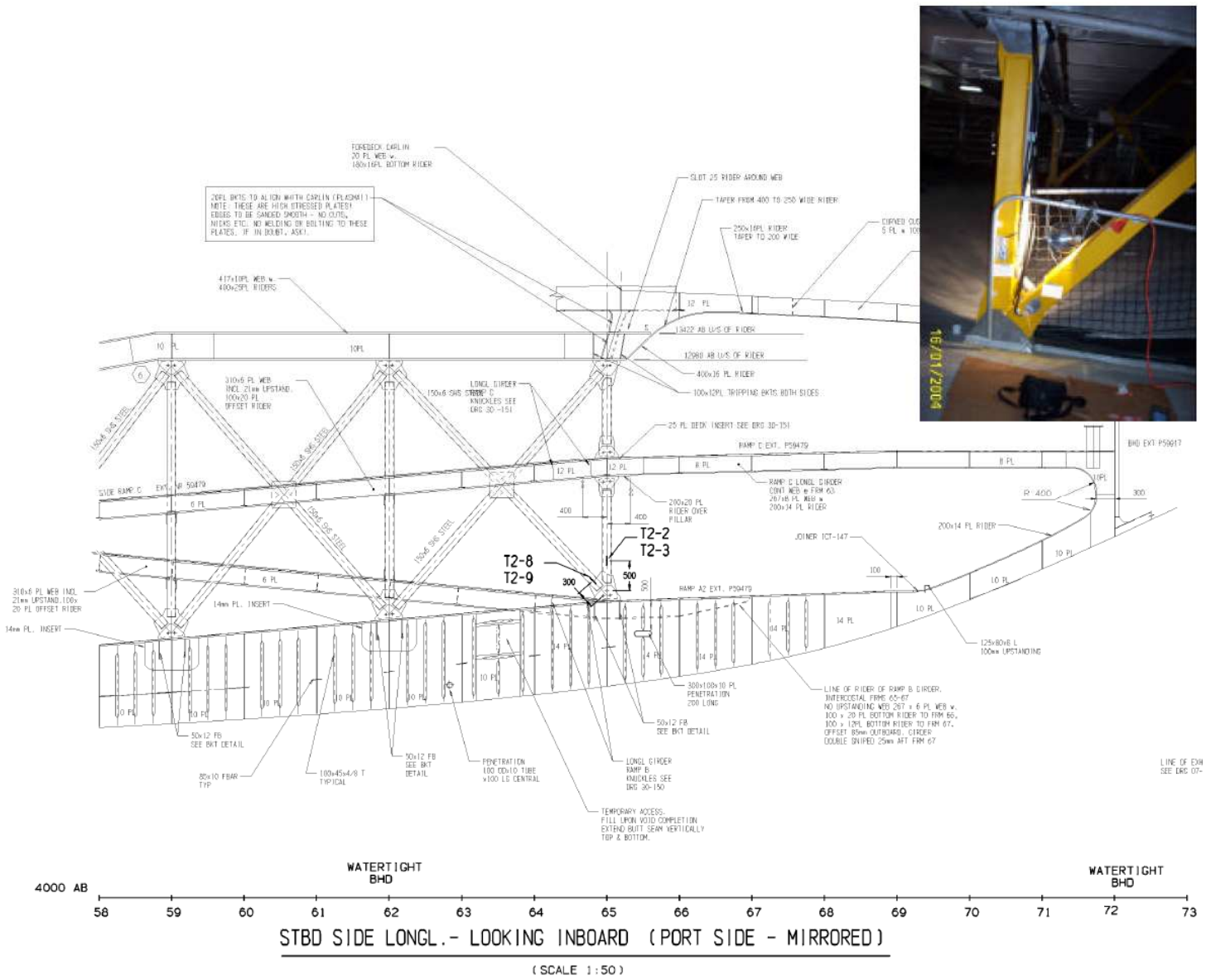

Figure 34: Layout of T2 sensors (view #3)

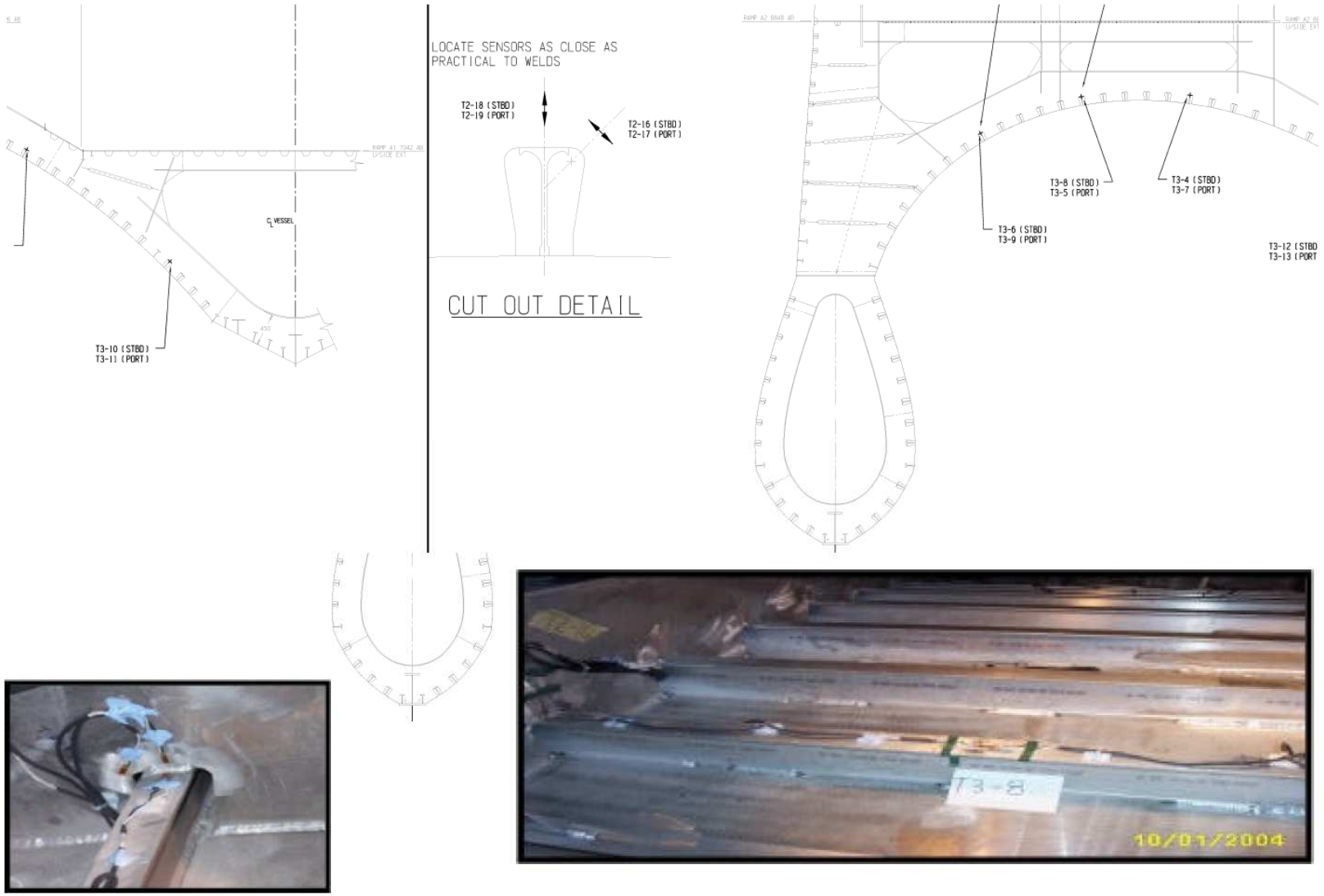

Figure 35: Layout of T2 sensors (view #4)

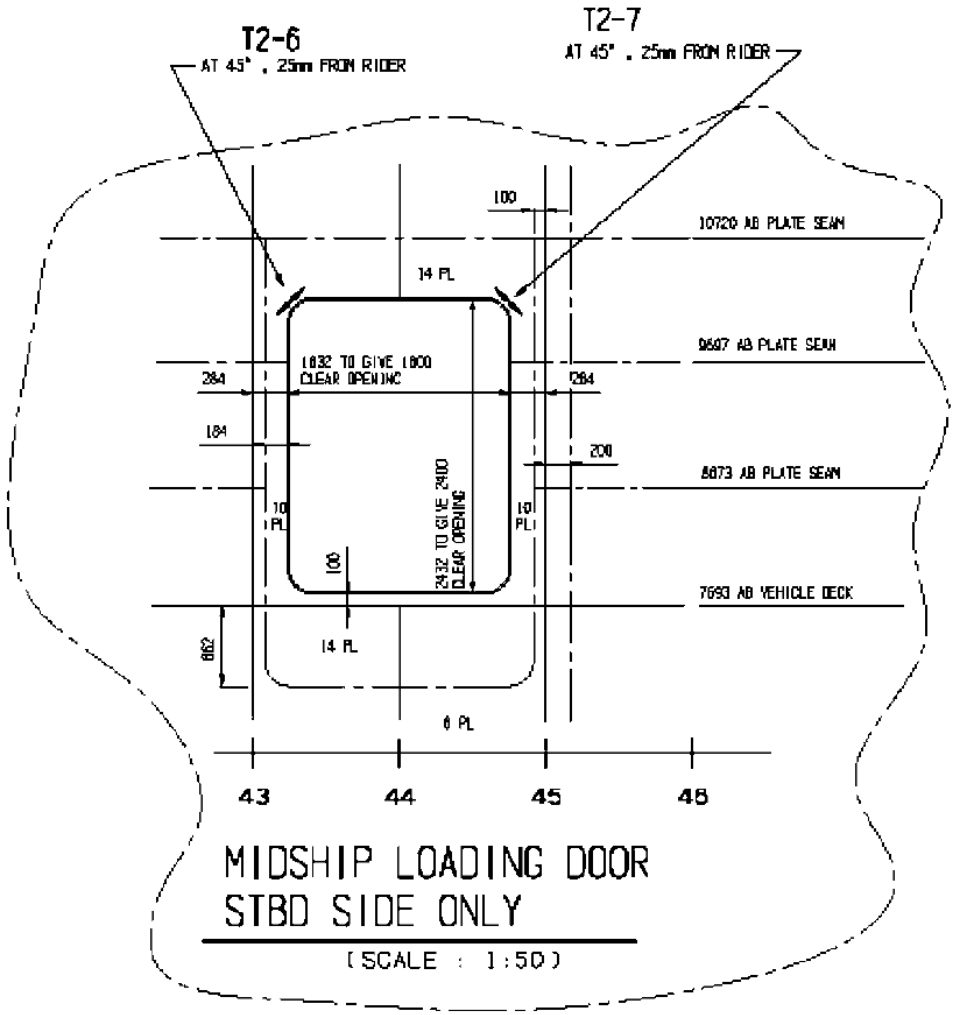

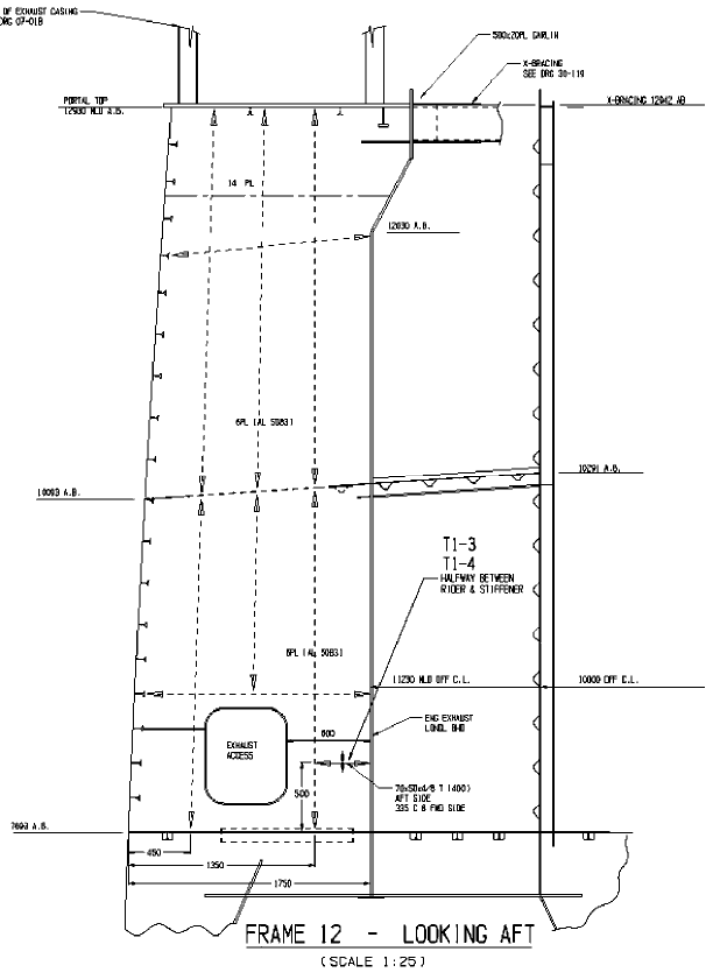

Figure 36: Layout of T1 and T2 sensors (view #1)

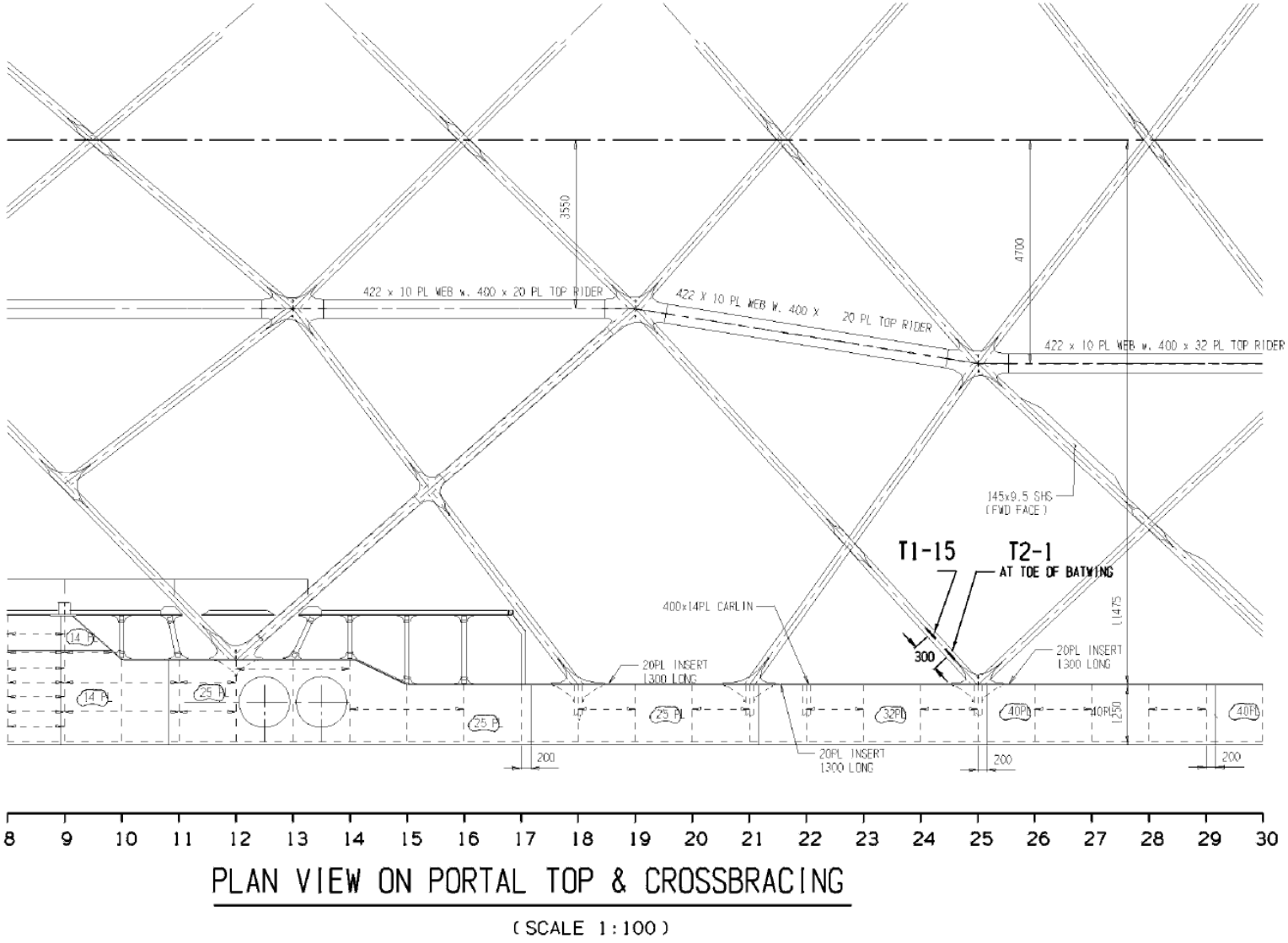

Figure 37: Layout of T1 and T2 sensors (view #2)

APPENDIX B

DEFINITION OF SEA STATES

Table 7: NATO sea states for open ocean, North Atlantic [2]

Sea State	Significant Wave Height		Modal Period	
	Range (ft)	Mean (ft)	Range (sec)	Mean (sec)
0-1	0.0 - 0.3	0.16	-	-
2	0.3 - 1.6	0.98	4.2 - 13.8	6.9
3	1.6 - 4.1	2.87	5.1 - 15.4	7.5
4	4.1 - 8.2	6.15	6.1 - 16.2	8.8
5	8.2 - 13.1	10.66	7.2 - 16.6	9.7

REFERENCES

[1] Brady, T.F., Bachman, R.J., Donnelly, M.J., and Griggs, D.B. (2004). "HSV-2 *Swift* Instrumentation and Technical Trials Plan," NSWCCD-65-TR-2004/18. Naval Surface Warfare Center, Carderock Division, West Bethesda, MD.

[2] Brady, T.F. (2004). "Global Structural Response Measurement of *Swift* (HSV-2) from JLOTS and Blue Game Rough Water Trials," NSWCCD-65-TR-2004/33. Naval Surface Warfare Center, Carderock Division, West Bethesda, MD.

[3] Brady, T.F., Gray, J.A., and Herda, A. (2004). "Wave Impact Loading Response Measurement and Analysis for HSV-2 from JLOTS and Blue Game Rough Water Trials," (NSWCCD-65-TR-2004/32). Naval Surface Warfare Center, Carderock Division, West Bethesda, MD.

[4] Salvino, L. W. and Collette, M. (2008). "Monitoring Marine Structures." *Encyclopedia of Structural Health Monitoring*, *Vol. 10*. C. Boller, F-K. Chang, Y. Fujino, eds. John Wiley & Sons, Chinchester, UK.

[5] Giurgiutiu, V. (2007). *Structural Health Monitoring with Piezoelectric Wafer Active Sensors*. Academic Press, Burlington, MA.

[6] Weaver, R.L. and Lobkis, O.I. (2001). "Ultrasonics without a source: thermal fluctuation correlations at MHz frequencies," *Physical Review Letters*, **87**, pp. 134301-1 – 134301-4.

[7] Larose, E., Roux P., and Campillo, M. (2007). "Reconstruction of Rayleigh-Lamb dispersion spectrum based on noise obtained from an air-jet forcing," *Journal of the Acoustical Society of America*, **122** (5), pp. 3437.

[8] Sabra, K.G., Srivastava A., Lanza di Scalea, F., Bartoli, I., Rizzo, P., and Conti S. (2008). "Structural health monitoring by extraction of coherent guided waves from diffuse fields," *Journal of the Acoustical Society of America*, **123** (1), pp. EL8-EL13.

[9] Farrar, C. and James, G. (1997). "System identification from ambient vibration measurements on a bridge," *Journal of Sound and Vibration*, **205**, pp. 1-18.

[10] Nagayama, T., Abe, M., Fujino, Y., and Ikeda, K. (2005). "Structural identification of a non-proportionally damped system and its application to a full-scale suspension bridge," *Journal of Structural Engineering*, **131** (10), 1536–1545.

[11] Sabra, K.G., Winkel, E.S., Bourgoyne, D.A., Elbing, B.R., Ceccio, S.L., Perlin, M. and Dowling, D.R. (2007). “On using cross-correlation of turbulent flow-induced ambient vibrations to estimate the structural impulse response. Application to structural health monitoring,” *Journal of the Acoustical Society of America*, **121** (4), pp. 1987-2005.

[12] Sabra, K.G., Roux, P. and Kuperman, W.A. (2005). “Emergence rate of the time domain Green’s function from the ambient noise cross correlation,” *Journal of the Acoustical Society of America*, **118** (6), pp. 3524-3531.

[13] Sabra, K.G., Gerstoft, P., Roux, P., Kuperman, W.A. and Fehler, M.C. (2005). “Surface wave tomography from microseisms in Southern California,” *Geophysical Research Letters*, **32**, L14311.

[14] Shapiro, N.M., Campillo, M., Stehly L., and Ritzwoller, M. (2005), “High resolution surface-wave tomography from ambient seismic noise,” *Science*, **307** pp. 1615–1618.

[15] Ha, Y.H., and Pearce, J.A. (1999). "A New Window and Comparison to Standard Windows," *IEEE Transactions on Acoustics, Speech, and Signal Processing*, **37** (2), pp. 298-301.

[16] Santamarina, J.C. and Fratta, D. (2005). *Discrete Signals and Inverse Problems: An Introduction for Engineers and Scientists*. Wiley, New York.